MCB
Journals.ASM.org

Increased BRAF Heterodimerization Is the Common Pathogenic Mechanism for Noonan Syndrome-Associated *RAF1* Mutants

Xue Wu,[a,b] Jiani Yin,[b] Jeremy Simpson,[d] Kyoung-Han Kim,[c]* Shengqing Gu,[a,b] Jenny H. Hong,[a] Peter Bayliss,[b] Peter H. Backx,[c] Benjamin G. Neel,[a,b] and Toshiyuki Araki[b]

Department of Medical Biophysics, University of Toronto, Toronto, Ontario, Canada[a]; Campbell Family Cancer Research Institute, Ontario Cancer Institute and Princess Margaret Hospital, University Health Network, Toronto, Ontario, Canada[b]; Department of Physiology and Medicine, Heart and Stroke/Richard Lewar Centre, University of Toronto, Toronto, Ontario, Canada[c]; and Department of Human Health and Nutritional Sciences, University of Guelph, Guelph, Ontario, Canada[d]

Noonan syndrome (NS) is a relatively common autosomal dominant disorder characterized by congenital heart defects, short stature, and facial dysmorphia. NS is caused by germ line mutations in several components of the RAS–RAF–MEK–extracellular signal-regulated kinase (ERK) mitogen-activated protein kinase (MAPK) pathway, including both kinase-activating and kinase-impaired alleles of *RAF1* (~3 to 5%), which encodes a serine-threonine kinase for MEK1/2. To investigate how kinase-impaired RAF1 mutants cause NS, we generated knock-in mice expressing *Raf1*^{D486N}. Raf1$^{D486N/+}$ (here D486N/+) female mice exhibited a mild growth defect. Male and female D486N/D486N mice developed concentric cardiac hypertrophy and incompletely penetrant, but severe, growth defects. Remarkably, Mek/Erk activation was enhanced in Raf1^{D486N}-expressing cells compared with controls. RAF1^{D486N}, as well as other kinase-impaired RAF1 mutants, showed increased heterodimerization with BRAF, which was necessary and sufficient to promote increased MEK/ERK activation. Furthermore, kinase-activating *RAF1* mutants also required heterodimerization to enhance MEK/ERK activation. Our results suggest that an increased heterodimerization ability is the common pathogenic mechanism for NS-associated *RAF1* mutations.

Noonan syndrome (NS) is a relatively common (1 in 1,000 to 2,500 live births) autosomal dominant disorder (28, 30, 45), characterized by short stature, craniofacial dysmorphia, a wide spectrum of congenital cardiac anomalies, and an increased risk of hematopoietic malignancy. Although NS is genetically heterogeneous (1, 4, 49), all known cases are caused by germ line mutations in conserved components of the canonical RAS–RAF–MEK–extracellular signal-regulated kinase (ERK) mitogen-activated protein kinase (MAPK) (here RAS/ERK) cascade, a key regulator of cell proliferation, differentiation, and survival (13, 24). Mutations in *PTPN11*, which encodes the protein tyrosine phosphatase SHP2, account for approximately one-half of NS cases (46). Other known NS genes include *SOS1* (~10%) (38, 47), *RAF1* (3 to 5%) (31, 36), *KRAS* (<2%) (41, 56), *NRAS* (9), and *SHOC2* (10) (<1 to 2%). Mutations in some of these genes, as well as in genes encoding other RAS/ERK pathway components, also cause phenotypically related disorders, such as neurofibromatosis type 1 (NF1), Costello syndrome, cardiofacio-cutaneous (CFC) syndrome, and LEOPARD syndrome (named for the major features of this disorder, including multiple lentigines, electrocardiographic conduction abnormalities, ocular hypertelorism, pulmonic stenosis, abnormal genitalia, retardation of growth, and sensorineural deafness); together with NS, these syndromes are now termed "RASopathies" (49). How mutations in the same signaling pathway cause similar yet clearly distinct phenotypes remains unclear. Consequently, a detailed understanding of RASopathy pathogenesis should yield new insights into RAS/ERK pathway regulation.

RAF family serine-threonine kinases (22, 25, 53) function as key RAS effectors, phosphorylating and activating the dual-specificity kinases MEK1 and MEK2, which in turn promote the activation of the MAPKs ERK1 and ERK2. The three mammalian RAF family members (RAF1, BRAF, and ARAF) differ in their expression profiles and regulatory mechanisms and have distinct roles during development. RAF1 (also known as CRAF) is the most intensively studied isoform. Nevertheless, controversy and disagreement surround the precise molecular events required for RAF1 activation, which include RAS-dependent membrane recruitment, conformational changes, dimerization or oligomerization, scaffold protein binding, and distinct phosphorylation/dephosphorylation events. RAF1 also has important kinase-independent functions. For example, it interacts with and inhibits apoptosis signal-regulating kinase 1 (ASK1) (5, 55), mammalian STE20-like kinase 2 (MST2) (29, 39), and Rok-α (32).

Two groups (31, 36) identified multiple missense mutations of *RAF1* in NS, which cluster in three regions. Approximately 70% of NS-associated *RAF1* alleles alter the motif flanking S259 within the so-called CR2 domain, which binds to 14-3-3 proteins and is critical for autoinhibition (21, 23). The second group of mutations (~15%) affects residues within the activation segment of the kinase domain (D486 and T491). The remaining alleles (~15%) involve two adjacent residues (S612 and L613) located C terminally to the kinase domain. Transient-transfection studies indicated that mutations affecting the 14-3-3 binding motif or the C terminus of the protein enhance RAF1 kinase activity and increase MEK/ERK activation in cells. In contrast, mutations that cluster in

Received 5 June 2012 Returned for modification 10 July 2012
Accepted 16 July 2012
Published ahead of print 23 July 2012
Address correspondence to Benjamin G. Neel, bneel@uhnresearch.ca, or Toshiyuki Araki, taraki@uhnres.utoronto.ca.
* Present address: Kyoung-Han Kim, Developmental and Stem Cell Biology, Hospital for Sick Children, Toronto, Ontario, Canada.

doi:10.1128/MCB.00751-12

TABLE 1 PCR primers

Purpose	Orientation	Sequence
PCR screening for 5′ loxP site	Sense	5′-TCCAGCTAATTGACATTGCCCGACAGACAGCTCAG-3′
	Antisense	5′-GAACGGGTTGTCATCCTGCATCCGGATTACTTCTG-3′
PCR screening and probe for Neo	Sense	5′-GGA TTG CAC GCA GGT TCT CCG-3′
	Antisense	5′-CGC CGC CAA GCT CTT CAG CAA-3′
5′ probe	Sense	5′-TGC TCT GGA GCT CAA ACC CTC AGT GTA G-3′
	Antisense	5′-CAT GGC TGA GTG GAC GGT CAG GCT G-3′
3′ probe	Sense	5′-GAG ACG GCA GAT CCT CAG TAG TAC TTG-3′
	Antisense	5′-ACG GTG GTA GTT GTG TCT TTG GCC ATG-3′
RT-PCR for Raf1 mRNA	Sense	5′-TCT CCA TGA AGG CCT CAC GGTG-3′
	Antisense	5′-AGA CTG GTA GCC TTG GGG ATG TAG-3′
PCR screening and genotyping for $Raf1^{D486N}$	Sense	5′-TGTGCGCATGCCATCGTTCCCTGTC-3′
	Antisense	5′-GCACCCTACTCTGGCCCAGTAATTC-3′

the activation segment are kinase impaired and reportedly act as dominant negative or null alleles (31, 36). Previous work suggested that the increased kinase activity of NS-associated CR2 domain mutants results from decreased S259 phosphorylation and consequent dissociation from 14-3-3 (20, 26, 31), but the mechanism underlying the increased kinase activity of the RAF1 C-terminal mutants remains unclear. Likewise, how kinase-defective RAF1 alleles cause NS has remained obscure, if not paradoxical. Studies of kinase-defective BRAF alleles strongly implicate enhanced MEK/ERK activation and heterodimerization with RAF1 in human melanoma pathogenesis (12, 51). The paradoxical activation of the MEK/ERK pathway in wild-type (WT) cells treated with selective small-molecule BRAF inhibitors has also been attributed to the ability of these inhibitors to induce BRAF/RAF1 heterodimer formation (14, 33). The relevance of these observations for *RAF1* alleles expressed at physiological expression levels remains to be determined.

Kinase-activating and kinase-impaired *RAF1* alleles are also associated with different syndromic phenotypes. NS patients with *RAF1* mutations have a much higher incidence (~75%) of hypertrophic cardiomyopathy (HCM) than is found in the overall NS population (~20%). However, only *RAF1* alleles encoding kinase-activated mutants are highly associated (~95%) with HCM. Recently, we reported that knock-in mice expressing the kinase-activated allele $Raf1^{L613V}$ develop typical NS features (short stature, facial dysmorphia, and hematological abnormalities) as well as HCM (54). As expected, agonist-evoked MEK/ERK activation was enhanced in multiple cell types expressing $Raf1^{L613V}$. Moreover, postnatal MEK inhibition normalized growth, facial, and cardiac defects in L613V/+ mice, showing that enhanced MEK/ERK activation is critical for evoking RAF1 mutant NS phenotypes.

Whether kinase-defective *Raf1* alleles also faithfully model human NS and, if so, how kinase-activating and kinase-defective mutants can cause similar phenotypes remain to be resolved. To investigate this paradox, we generated and analyzed knock-in mice expressing kinase-impaired NS mutant $Raf1^{D486N}$ and also reexamined the effects of various other NS mutants expressed at more physiological levels than in previous transient-transfection studies. Our results strongly implicate an increased heterodimerization ability as the common pathogenic mechanism for NS-associated *RAF1* mutations.

MATERIALS AND METHODS

Generation of $Raf1^{D486N}$ knock-in mice. To construct the targeting vector for our inducible $Raf1^{D486N}$ knock-in mice, a "short arm," containing *Raf1* exon 12 (SacII-NotI genomic fragment), and a "long arm," which includes exons 13 to 16 (BamHI-ClaI genomic fragment), were ligated into the vector pGK-Neo-HSV-1 TK (42). The D486N (exon 16) mutation, marked by a unique ApoI site, was introduced by site-directed mutagenesis. A splice acceptor sequence, a *Raf1* cDNA fragment encoding wild-type exons 13 to 16, and a pGK-Neo (Neo) gene were positioned after the first LoxP site as a SalI-XbaI fragment. The targeting vector was linearized with SacII and electroporated into G4 embryonic stem (ES) cells (129Sv × C57BL/6 F1 background). Genomic DNA, isolated from doubly G418/1-(2-deoxy-2-fluoro-β-D-arabinofuranosyl)-5 iodouracil (FIAU)-resistant (positive and negative selection, respectively) ES clones, was screened by PCR using primers outside and inside the targeting vector (Table 1). Homologous recombinants were confirmed by Southern blotting using Neo and external (5′ and 3′) probes (Table 1). For these experiments, genomic DNA was digested with XbaI (5′ and Neo probes) or BamHI (3′ probe).

To validate the desired properties of the targeted locus, correctly targeted ES cells were transfected with a Cre-expressing plasmid (pMSCV-GFP-Cre) to excise the cDNA-Neo cassette (see below for detailed methods). The expression of $Raf1^{D486N}$ mRNA was confirmed by reverse transcription (RT)-PCR (Table 1), followed by digestion with ApoI, which marks the D486N allele. Chimeras were generated by outbred morula aggregation (Toronto Centre of Phenogenomics), and germ line transmission was obtained (D486Nfl/+ mice). D486Nfl/+ mice (129Sv × C57BL/6 background) were crossed to EIIa-Cre (129Sv) mice, which express Cre ubiquitously, and then to WT (C57BL/6) mice to generate mice with global $Raf1^{D486N}$ expression (D486N/+ mice; 129Sv × C57BL/6). Mice on a 129Sv × C57BL/6 mixed background were used for all experiments. For genotyping, genomic DNA was prepared from tails and then subjected to PCR (Table 1) and digestion with ApoI.

All animal studies were approved by the University Health Network Animal Care Committee (Toronto, Ontario, Canada) and performed in accordance with the standards of the Canadian Council on Animal Care.

Cell culture. ES cells were cultured on γ-irradiated mouse embryonic fibroblast (MEF) feeders in knockout Dulbecco's modified Eagle's medium (DMEM) (Invitrogen) containing 15% ES cell-tested (HyClone; Thermo Scientific) fetal bovine serum (FBS), 2 mM L-glutamine (Invit-

rogen), 0.1 mM nonessential amino acids (NEAA) (Invitrogen), 0.1 mM β-mercaptoethanol (Sigma), 100 U/ml penicillin-streptomycin (Invitrogen), and 500 U/ml leukemia inhibitory factor (LIF) (ESGro; Chemicon). ES cells were transfected with a murine stem cell virus (MSCV)-green fluorescent protein (GFP)-Cre plasmid using Lipofectamine 2000 reagent (Invitrogen) according to the manufacturer's protocol. GFP-positive cells were purified by fluorescence-activated cell sorting (FACS) at 48 h posttransfection and then used for RNA isolation.

Primary MEFs were prepared from embryonic day 13.5 (E13.5) embryos and cultured in DMEM (Wisent Inc.) containing 10% FBS (Wisent Inc.) and 100 units/ml penicillin-streptomycin (Invitrogen), as described previously (57). MEFs were starved in serum-free DMEM for 16 h before stimulation and then stimulated with epidermal growth factor (EGF) (PeproTech) before harvesting. Primary MEFs were immortalized by the 3T3 protocol (50). Immortalized MEFs were cultured in DMEM containing 10% FBS and 100 units/ml penicillin-streptomycin.

Neonatal mouse ventricular myocytes (neonatal cardiomyocytes) were isolated by using methods adapted from those reported by a previous study (58). In brief, 1-day-old mouse hearts were harvested and predigested with 0.15 mg/ml trypsin (Invitrogen) at 4°C for 12 to 16 h, followed by 50 U/ml type II collagenase (Worthington Biochemical) and 0.2 mg/ml trypsin in calcium- and bicarbonate-free Hanks buffer with HEPES for 1 to 2 h at 37°C. Noncardiomyocytes were depleted by differential plating for 1 h. Cardiomyocytes were counted, seeded at 2.5×10^5 cells/ml on Falcon Primaria tissue culture plates (BD Biosciences), and cultured at 37°C in DMEM–Ham's F-12 medium (1:1 [vol/vol]; Invitrogen), 10% FBS, and 100 U/ml penicillin-streptomycin (Invitrogen) supplemented with 0.1 mM bromodeoxyuridine (Sigma-Aldrich) and 20 μM arabinosylcytosine (Sigma-Aldrich) to inhibit rapidly proliferating cells. After 24 h, this medium was replaced with serum-free DMEM–Ham's F-12 (1:1) medium supplemented with 1% insulin-transferrin-selenium-X supplements (Invitrogen). After an additional 24 h, cardiomyocytes were stimulated with 10 ng/ml interleukin-6 (IL-6; PeproTech), 1 μg/ml angiotensin II (Ang-II; Sigma-Aldrich), 100 ng/ml insulin-like growth factor I (IGF-I; PeproTech), 50 ng/ml EGF (PeproTech), or 100 ng/ml NRG (heregulin β1; PeproTech) before harvesting.

Noncardiomyocytes from the above-described preparation, comprising mainly cardiac fibroblasts, were cultured in DMEM containing 10% FBS and 100 units/ml penicillin-streptomycin. Cardiac fibroblasts were starved in serum-free DMEM for 16 h and then stimulated with EGF (50 ng/ml), IGF-I (100 ng/ml), platelet-derived growth factor (PDGF) (100 ng/ml), or fibroblast growth factor 2 (FGF2) (100 ng/ml), all from PeproTech, before harvesting.

Flp-In T-REx 293 cell lines were cultured in DMEM (Wisent Inc.) containing 10% tetracycline-tested Gibco FBS (Invitrogen) and 100 units/ml penicillin-streptomycin (Invitrogen). To induce the expression of the indicated gene, a final concentration of 1 μg/ml tetracycline (Sigma-Aldrich) was added to the cells, followed by incubation for 24 h before harvesting for analysis.

Generation of Flp-In T-REx 293 expression cell lines. *RAF1* mutations were introduced into a Flag-tagged human *RAF1* construct (a gift from Bruce Gelb, Mt. Sinai Hospital, New York, NY) by site-directed mutagenesis. Flag-tagged human WT or mutant *RAF1* coding sequences were cloned into the KpnI and XhoI restriction sites of the vector pcDNA5/FRT/TO (Invitrogen). Flp-In T-REx 293 host cells (Invitrogen) were cotransfected with pOG44 (Invitrogen) and pcDNA5/FRT/TO expression plasmid DNAs, using FuGENE HD transfection reagent (Promega) according to the manufacturer's protocol. Hygromycin-resistant colonies were picked and expanded to assay for the tetracycline-regulated expression of Flag-RAF1.

Inducible RAF1/BRAF heterodimerization. Inducible RAF1/BRAF heterodimerization was achieved by using the Argent regulated heterodimerization kit (Ariad). A Flag-tagged human $RAF1^{R401H/D486N}$ cDNA was cloned into the EcoRI and XbaI restriction sites of the vector pC_4EN-F1. A human *BRAF* cDNA was cloned into the XbaI restriction site of the vector pC_4-R_HE. The resultant FKBP and FRB fusion protein constructs were cotransfected into Flp-In T-REx 293 host cells, using FuGENE HD transfection reagent (Promega) as described above.

Lentivirus production and transduction. Lentiviral short hairpin RNA (shRNA) expression plasmids (hairpin-pLKO.1) were obtained from Jason Moffat (University of Toronto). shRNA oligonucleotide sequences against murine *Braf* (5′-CCACATCATTGAGACCAAATT-3′ or 5′-CGAGGATACCTATCTCCAGAT-3′) and murine *Araf* (5′-CAGGCTCATCAAAGGAAGAAA-3′) and a control shRNA against luciferase (5′-CAAATCACAGAATCGTCGTAT-3′) were used. To generate lentiviruses, 2×10^6 293T packaging cells in growth medium (DMEM plus 10% FBS) were transfected with 3 μg lentiviral shRNA construct, 2.7 μg packaging plasmid (pCMV-dR8.91), and 0.3 μg envelope plasmid (vesicular stomatitis virus G protein [VSV-G]) in 10-cm cell culture plates, using FuGENE HD transfection reagent (Promega) according to the manufacturer's protocol. Transfection medium was changed on the following morning and replaced with 10 ml high-serum growth medium (DMEM plus 30% FBS) for viral harvest. Virus-containing supernatants were collected at 48 h posttransfection, subsequently passed through a 0.45-μm filter to remove cell debris, aliquoted, and stored at −80°C.

For knockdown experiments, cells were transduced in 10-cm plates with 1 ml virus in the presence of 6 μg/ml Polybrene for 24 h, followed by selection with 2.5 μg/ml puromycin for 48 h. After puromycin selection, transduced cells were replated for biochemical analysis.

Retrovirus production and transduction. A Myc epitope tag was added to the N terminus of human *BRAF* cDNA (The Centre for Applied Genomics) by using PCR. The $BRAF^{R509H}$ mutation was introduced by site-directed mutagenesis. RNA interference (RNAi)-insensitive $BRAF^{WT}$ and $BRAF^{R509H}$ mutants were generated by introducing three silent mutations into the shRNA target sequence in *BRAF* by site-directed mutagenesis. The blunt-ended *Myc-*$BRAF^{WT}$ or *Myc-*$BRAF^{R509H}$ coding sequence was cloned into the blunt-ended XhoI site of the pMSCV-IRES-EGFP vector upstream of the internal ribosome entry site (IRES) sequence.

To generate retroviruses, 1×10^6 293T packaging cells in growth medium (DMEM plus 10% FBS) in 6-cm cell culture plates were transfected with 3 μg retroviral plasmid pMSCV and 3 μg EcoPac packaging plasmid using FuGENE HD transfection reagent (Promega) according to the manufacturer's protocol. Transfection medium was changed on the following morning and replaced with 5 ml fresh growth medium for viral harvest. Virus-containing supernatants were collected at 48 h posttransfection and passed through a 0.45-μm filter to remove cell debris. MEFs were transduced in 15-cm plates with 5 ml virus in the presence of 6 μg/ml Polybrene for 24 h, followed by FACS analysis to select for GFP-positive cells.

Biochemical analysis. Total protein extracts from cells or tissues were prepared in radioimmunoprecipitation assay (RIPA) buffer (50 mM Tris-HCl [pH 7.5], 150 mM NaCl, 2 mM EDTA, 1% NP-40, 0.5% Na deoxycholate, 0.1% SDS) containing a protease and phosphatase inhibitor cocktail (40 μg/ml phenylmethylsulfonyl fluoride [PMSF], 20 mM NaF, 1 mM Na_3VO_4, 10 mM β-glycerophosphate, 10 mM sodium pyrophosphate, 2 μg/ml antipain, 2 μg/ml pepstatin A, 20 μg/ml leupeptin, and 20 μg/ml aprotinin). Lysates (10 to 25 μg protein) were resolved by SDS-PAGE and analyzed by immunoblotting.

For immunoprecipitations, total cell extracts were prepared in NP-40 buffer (20 mM Tris-HCl [pH 8.0], 137 mM NaCl, 2 mM EDTA, 1% NP-40, 10% glycerol) containing the protease and phosphatase inhibitor cocktail described above. Lysates were incubated with anti-Raf1 antibodies (BD Biosciences) and protein G-Sepharose 4 Fast Flow (GE Healthcare) or anti-Flag M2 affinity agarose gel (Sigma-Aldrich) for 3 h at 4°C with rotation. Beads were washed four times with NP-40 buffer, and immunoprecipitates were analyzed by immunoblotting.

Antibodies for immunoblots included antibodies to RAF1 (BD Biosciences), Flag tag M2 (Sigma-Aldrich), ERK2 (D2), Braf (H145), and Araf (H70) from Santa Cruz Biotechnology Inc.; ERK1/2 from Millipore; and phospho-MEK1/2, MEK1/2, phospho-p44/42 MAPK, and phospho-

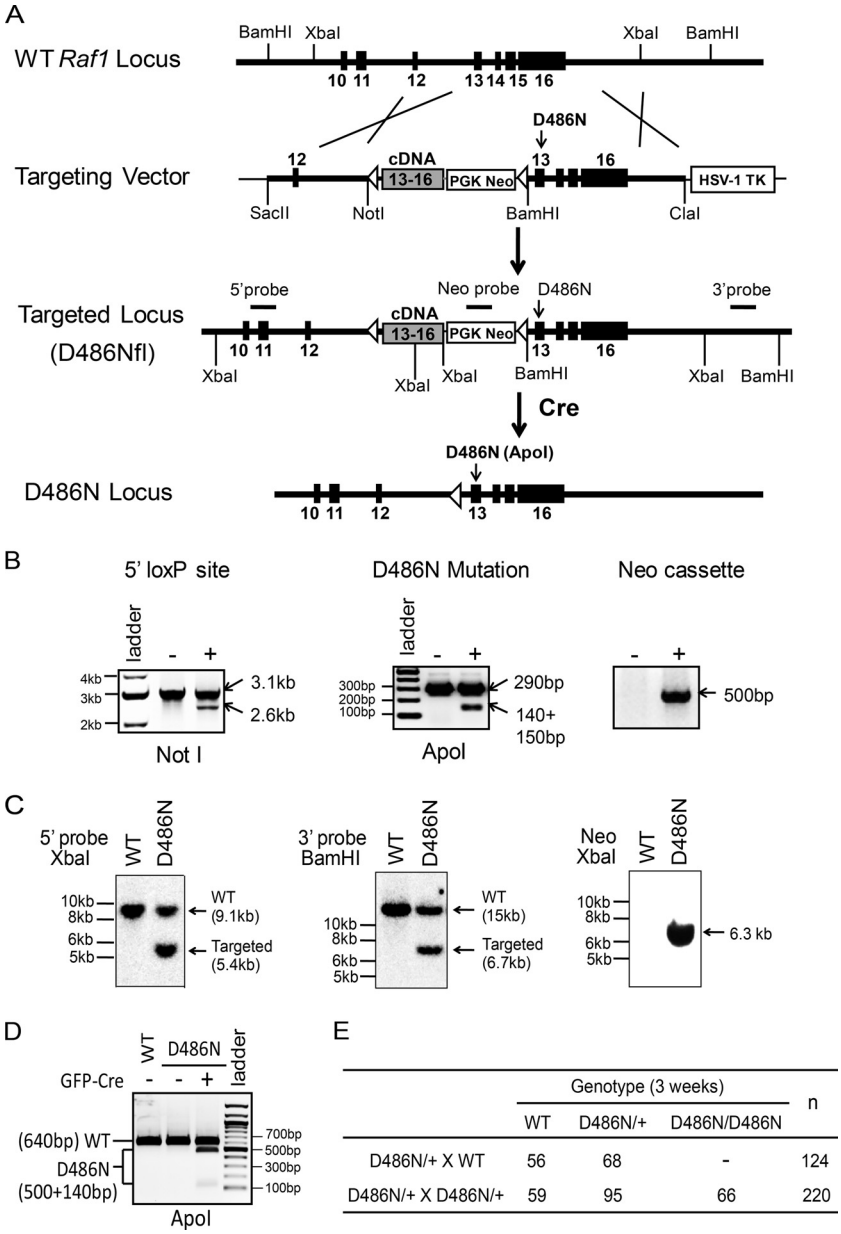

	Genotype (3 weeks)			n
	WT	D486N/+	D486N/D486N	
D486N/+ X WT	56	68	-	124
D486N/+ X D486N/+	59	95	66	220

FIG 1 Generation of *Raf1*^{D486N} knock-in mice. (A) Targeting strategy. Structures of the *Raf1* locus, targeting vector, and mutant allele and the location of probes for Southern blotting are shown. (B) Selection of targeted ES cells. To assay for the inclusion of the 5′ LoxP site, a PCR product, obtained by using primers within exon 11 and the *Raf1* cDNA, was digested with NotI. To ensure the inclusion of the D486N mutation, a PCR product, obtained by using primers around exon 13, was digested with ApoI. To assay for the inclusion of the Neo cassette, a PCR product was obtained by using primers within the pGK-Neo gene. (C) ES cells are targeted correctly. Genomic DNA from WT ES cells and PCR-positive D486Nfl/+ ES clones was digested with XbaI (5′ and Neo probes) or BamHI (3′ probe) and subjected to Southern blotting with 5′, 3′, or Neo probes. (D) Inducible expression of the *Raf1*^{D486N} allele. RNA was isolated from WT and D486Nfl/+ ES cells with or without the prior transfection of plasmid pMSCV-GFP-Cre and reverse transcribed. A PCR product, obtained by using primers within exon 11 and at the end of exon 16 of the *Raf1* cDNA, was digested with ApoI. Note that the mutant allele is silent until Cre is introduced and is then expressed efficiently. (E) Progeny from D486N/+ matings with the indicated littermates.

RAF1-Ser289/296/301 from Cell Signaling Technology. Primary antibody binding was visualized by IRDye infrared secondary antibodies using the Odyssey Infrared imaging system (Li-Cor Biosciences). Quantification was performed by using Odyssey V3.0 software.

Body size analysis and morphometry. Body length (anal-nasal [AN] length) and weight were measured weekly. For skeletal morphometry, mice were anesthetized with 2% isoflurane and scanned by using a Locus Ultra micro-computed tomography (microCT) scanner (GE Healthcare). Three-dimensional images of the skeleton were generated and analyzed with GEHC MicroView software (GE Healthcare). Skull measurements were done as described on the Jackson Laboratory website (http://craniofacial.jax.org/standard_protocols.html).

Echocardiographic measurements. Echocardiography was performed as described previously (54). In brief, mice were anesthetized with isoflurane-oxygen (2% to 100%), and body temperature was maintained at ~37.5°C. Transthoracic two-dimensional (2D) and M-mode echocardiography was performed from the long-axis view of the heart at the level of the papillary muscle with a Visualsonics Vevo 770 imaging system

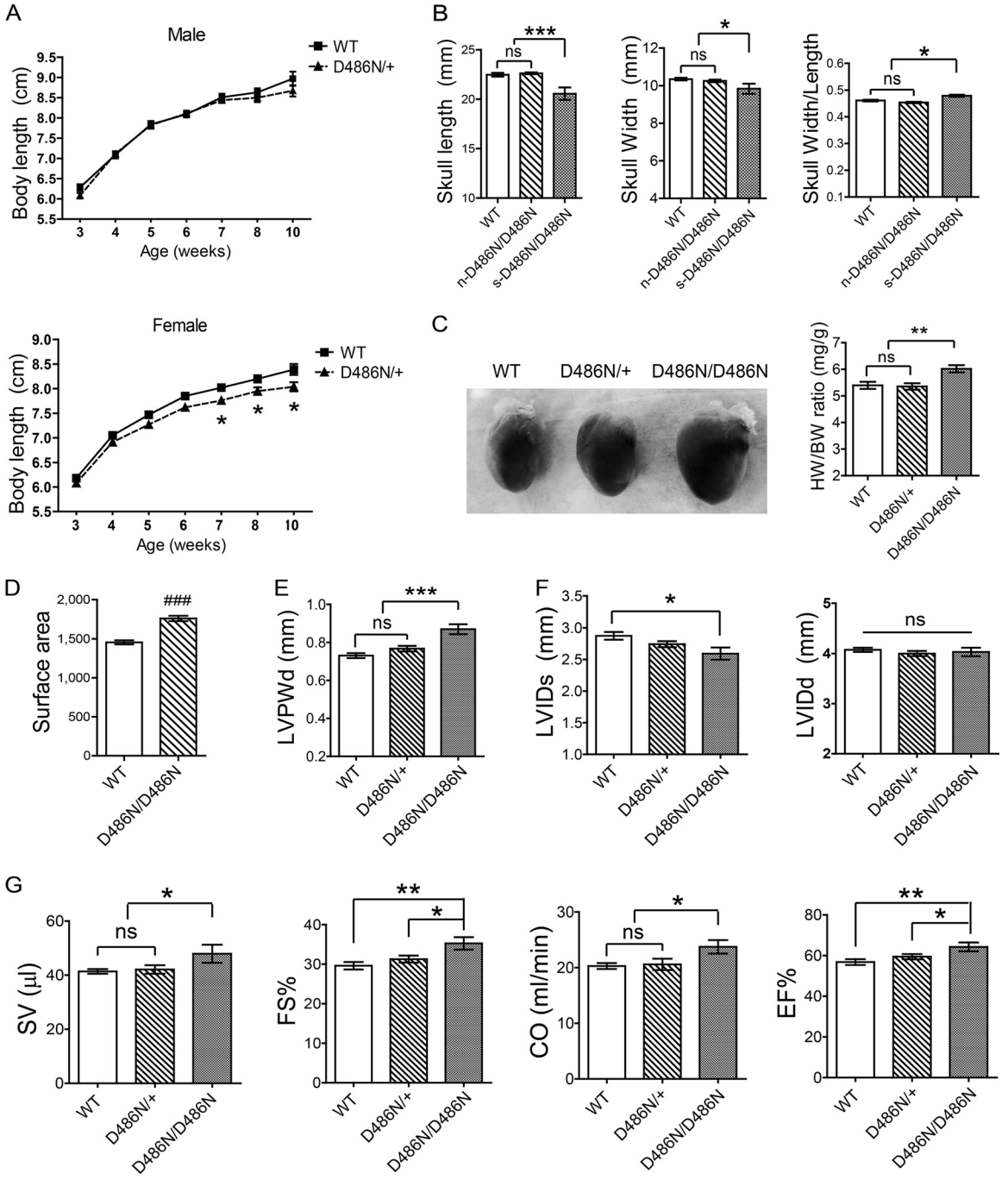

FIG 2 Phenotypes of D486N/+ and D486N/D486N mice. (A) D486N/+ females have a mild growth defect. Shown are growth curves of male (top) and female (bottom) ($P < 0.0001$, determined by two-way repeated-measure ANOVA) WT ($n = 25$) and D486N/+ ($n = 25$) mice. (B) D486N/D486N mice with severe growth defect (s-D486N/D486N) have facial dysmorphia. Shown are morphometric measurements from microCT scans of a cohort of 2-month-old WT ($n = 12$), normal-sized D486N/D486N (n-D486N/D486N) ($n = 10$), and s-D486N/D486N ($n = 3$) male mice. (C) Representative gross appearance and heart weight/body weight (mg/g) ratios of WT ($n = 15$), D486N/+ ($n = 20$), and D486N/D486N ($n = 15$) male mice at 4 months. (D) Surface area of isolated neonatal cardiomyocytes from WT and D486N/D486N mice. For each genotype, 350 cells were analyzed by using ImageJ. ###, $P < 0.001$, determined by a 2-tailed Student t test. (E) Left ventricular diastolic posterior wall thickness (LVPWd) at 4 months, measured by echocardiography ($n = 12$ for WT mice, $n = 20$ for D486N/+ mice, and $n = 12$ for D486N/D486N mice). (F) Left ventricular chamber dimensions of 4-month-old WT ($n = 12$), D486N/+ ($n = 20$), and D486N/D486N ($n = 12$) hearts. LVIDs, left ventricular internal end-systolic dimension; LVIDd, left ventricular internal end-diastolic dimension. (G) Echocardiographic parameters of 4 month-old WT ($n = 12$), D486N/+ ($n = 20$), and D486N/D486N ($n = 12$) hearts. SV, stroke volume; FS, fractional shortening; CO, cardiac output; EF, ejection fraction. *, $P < 0.05$; **, $P < 0.01$; ***, $P < 0.001$ (determined by a Bonferroni posttest when ANOVA was significant); ns, not significant.

(Visualsonics) equipped with a 30-MHz linear transducer (RMV707B). Measurements of the left ventricular (LV) internal end-systolic dimension (LVIDs), the LV internal end-diastolic dimension (LVIDd), and the LV diastolic posterior wall thickness (LVPWd) were made under time motion (TM) mode.

Statistics. All data are presented as means ± standard errors of the means (SEM). Statistical significance was evaluated by using Student's *t* test, a one-way analysis of variance (ANOVA), or a two-way repeated-measure ANOVA, as appropriate. If the ANOVA was significant, individual differences were evaluated by using the Bonferroni posttest. All statistical analyses were performed with GraphPad Prism 5. For all studies, a P value of <0.05 was considered significant.

RESULTS

Generation of *Raf1*^{D486N} mice. To avoid the possibility that the expression of kinase-impaired Raf1 might cause embryonic lethality, we designed an inducible *Raf1*^{D486N} "knock-in" allele (D486Nfl) (Fig. 1A). The targeting vector included a cassette containing a splice acceptor sequence, a *Raf1* cDNA fragment encoding WT exons 13 to 16, and a pGK-Neo gene. The fusion cDNA/Neo cassette was flanked by LoxP sites and was positioned between *Raf1* exons 12 and 13, with the D486N mutation introduced into exon 13 and a herpes simplex virus thymidine kinase (HSV-TK) cassette for negative selection. In the absence of Cre recombinase (Cre), *Raf1* exon 12 should be spliced to the cDNA (exons 13 to 16), resulting in the expression of WT *Raf1*. When Cre is present, the floxed cassette is excised, leading to the transcription of the mutant *Raf1* allele (D486N).

The targeting construct was electroporated into G4 ES cells, and correctly targeted clones (D486Nfl/+) were identified by PCR (Fig. 1B) and confirmed by Southern blotting (Fig. 1C). To test whether the mutant *Raf1* allele could be induced in D486Nfl/+ ES cells, a Cre expression vector (pMSCV-GFP-Cre) was introduced; as expected, this resulted in the efficient transcription of the mutant allele (Fig. 1D). Chimeras were generated by outbred morula aggregation, and germ line transmission was obtained. D486Nfl/+ progeny were crossed to EIIa-Cre mice, which express Cre ubiquitously, and then to WT mice, thereby generating mice with global *Raf1*^{D486N} expression (referred to as D486N/+ mice) on a 129Sv × C57BL/6 mixed background. D486N/+ littermates were intercrossed to generate mice homozygous for *Raf1*^{D486N} (referred to as D486N/D486N mice). D486N/+ and D486N/D486N mice were obtained at the expected Mendelian ratios at weaning (Fig. 1E), indicating that *Raf1*^{D486N} expression is compatible with embryonic development.

Phenotypes of D486N/+ and D486N/D486N mice. Major features of NS include short stature, facial dysmorphia, cardiovascular abnormalities, and often some form of myeloproliferative disease (MPD) (44). D486N/+ female mice exhibited a mild but reproducible growth defect compared with their WT littermates, although male heterozygotes had a normal body size (Fig. 2A). Male and female D486N/D486N mice showed two distinct patterns of growth: about two-thirds of these animals had a normal growth pattern, but in the remaining one-third, body length and weight were markedly decreased (~50% smaller than littermate controls). Here, we refer to the normal-sized mice as n-D486N/D486N mice and the smaller ones as s-D486N/D486N mice. The majority of s-D486N/D486N mice died shortly after weaning, while those that survived continued to have a reduced body size and a hunched appearance with ruffled fur and frequent tremors

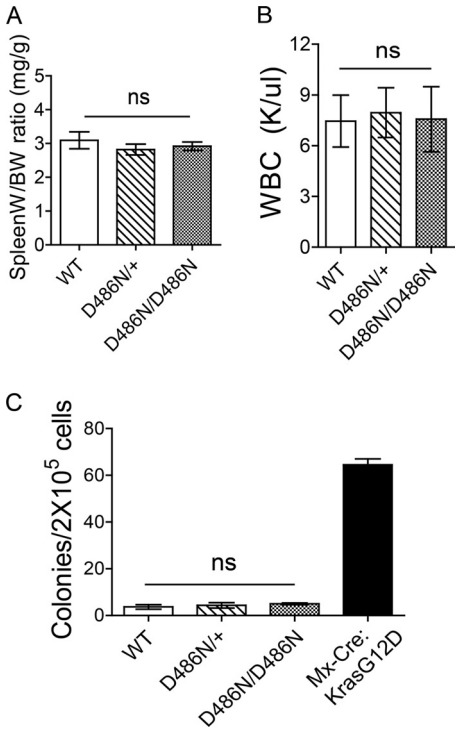

FIG 3 Additional phenotyping of D486N/+ and D486N/D486N mice. (A) Spleen weight/body weight (SpleenW/BW) ratios of WT, D486N/+, and D486N/D486N male mice at 5 months ($n = 15$ for each genotype). (B) White blood cell (WBC) counts in WT, D486N/+, and D486N/D486N male mice at 1 year ($n = 6$ for each genotype). (C) Myeloid colony formation in the absence of cytokines of bone marrow cells from WT, D486N/+, and D486N/D486N mice. Bulk bone marrow cells were extracted at 1 year ($n = 3$ for each genotype). Colonies were enumerated 7 days after plating. Bone marrow from an induced Mx-Cre:KrasG12D mouse ($n = 1$) served as a positive control for cytokine-independent colony formation. ns, not significant.

and ultimately died between 4 and 8 months of age (data not shown). Consistent with their decreased body size, the skulls of s-D486N/D486N mice were significantly shorter than those of WT mice. However, the skull width was decreased only slightly, resulting in a significant increase in the width/length ratio and a "triangular" facial appearance (Fig. 2B and data not shown). In contrast, n-D486N/D486N mice had normal life span, body size, and facial morphology (Fig. 2B and data not shown). Because D486N/D486N mice were maintained on a mixed-strain background, genetic modifiers presumably account for the variable phenotype.

Similar to *RAF1*$^{D486N/+}$ NS patients, D486N/+ mice had a normal heart size. In contrast, n-D486N/D486N mice showed cardiac enlargement, manifested by a significantly increased heart weight/body weight ratio compared with those of their WT and D486N/+ littermates (Fig. 2C). Neonatal cardiomyocytes prepared from D486N/D486N mice showed a significantly increased surface area compared with that of WT cardiomyocytes, indicating that cardiac enlargement was due to hypertrophy (Fig. 2D). Echocardiography performed on 4-month-old n-D486N/D486N mice showed an increased left ventricular diastolic posterior wall thickness (LVPWd), as expected, while D486N/+ mice had a normal LVPWd (Fig. 2E). In contrast to *Raf1*$^{L613V/+}$ mice, which developed cardiac dilatation (54), the left ventricular internal end-dia-

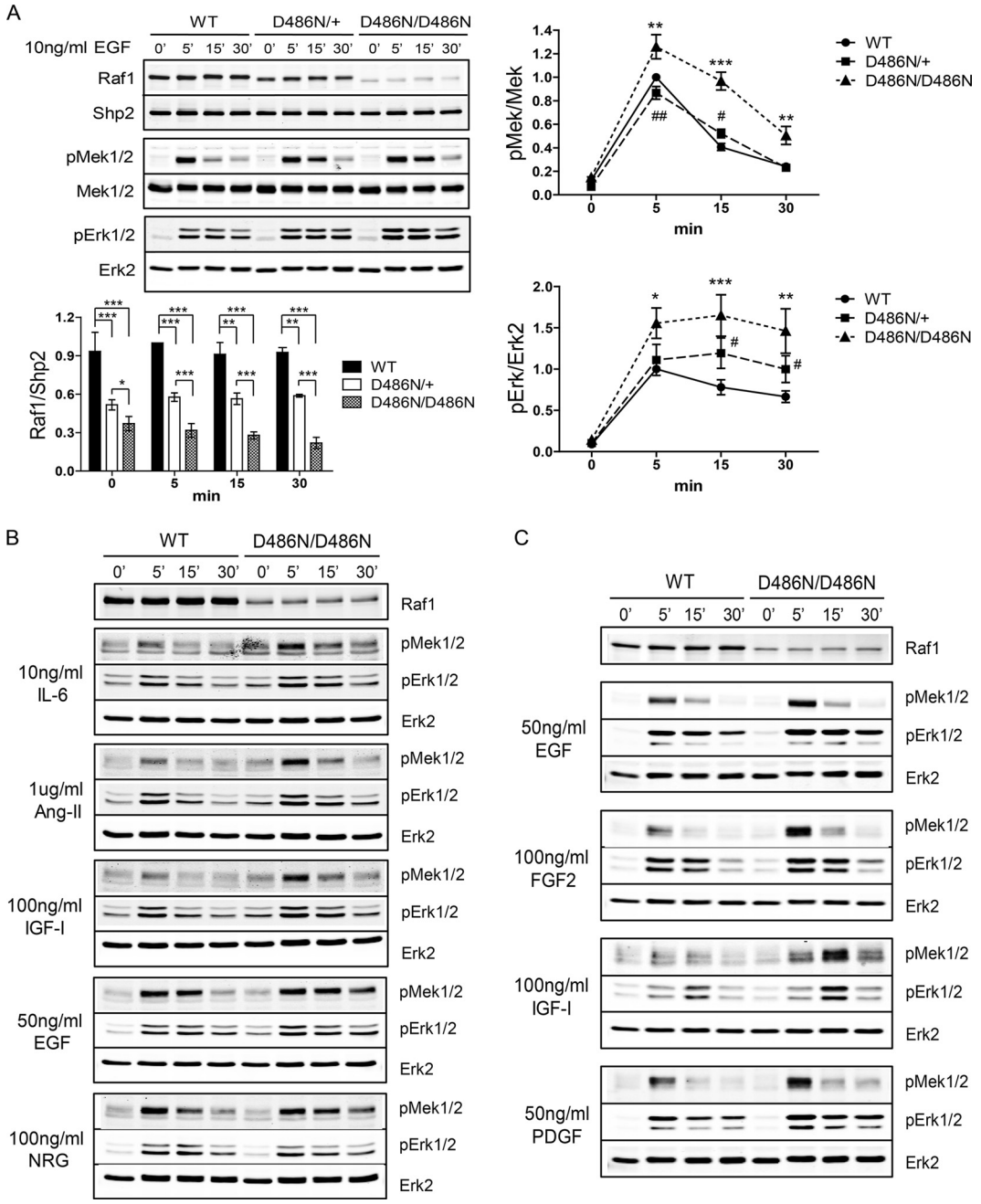

FIG 4 The Raf1^{D486N} mutant increases Mek and Erk activation. (A) Primary mouse embryonic fibroblasts (MEFs) from WT, D486N/+, and D486N/D486N mice were serum starved for 16 h and then stimulated with EGF for the indicated times. Cell lysates were immunoblotted with the indicated antibodies. A representative blot and quantification of blots from all experiments are shown ($n = 6$; two independent experiments using three different MEF strains). *, $P < 0.05$; **, $P < 0.01$; ***, $P < 0.001$ (left bottom). *, $P < 0.05$; **, $P < 0.01$; ***, $P < 0.001$ (right) (D486N/D486N versus WT). #, $P < 0.05$; ##, $P < 0.01$ (right) (D486N/+ versus WT) (determined by a Bonferroni posttest when ANOVA was significant). (B) Neonatal cardiomyocytes from WT and D486N/D486N mice were starved for 24 h and then stimulated for the indicated times with the indicated agonists. Ang-II, angiotensin II; NRG, heregulin β1. Cell lysates were immunoblotted as indicated. (C) Cardiac fibroblasts from WT and D486N/D486N neonates were starved for 16 h and then stimulated with various agonists for the indicated times. Cell lysates were immunoblotted with the indicated antibodies.

stolic dimension (LVIDd) remained normal in D486N/+ and n-D486N/D486N mice, while the left ventricular internal end-systolic dimension (LVIDs) tended to be reduced in D486N/+ hearts and was decreased significantly in n-D486N/D486N hearts (Fig. 2F). Stroke volume (SV), fractional shortening (FS), cardiac output (CO), and ejection fraction (EF) were also increased in n-D486N/D486N mice (Fig. 2G). Cardiac parameters could not be assessed for s-D486N/D486N mice because of their size and generally poor health. Overall, these findings indicate that D486N/D486N mice have concentric cardiac hypertrophy with enhanced cardiac function.

Unlike other mouse models of NS (2, 3, 6, 54), D486N/+ and

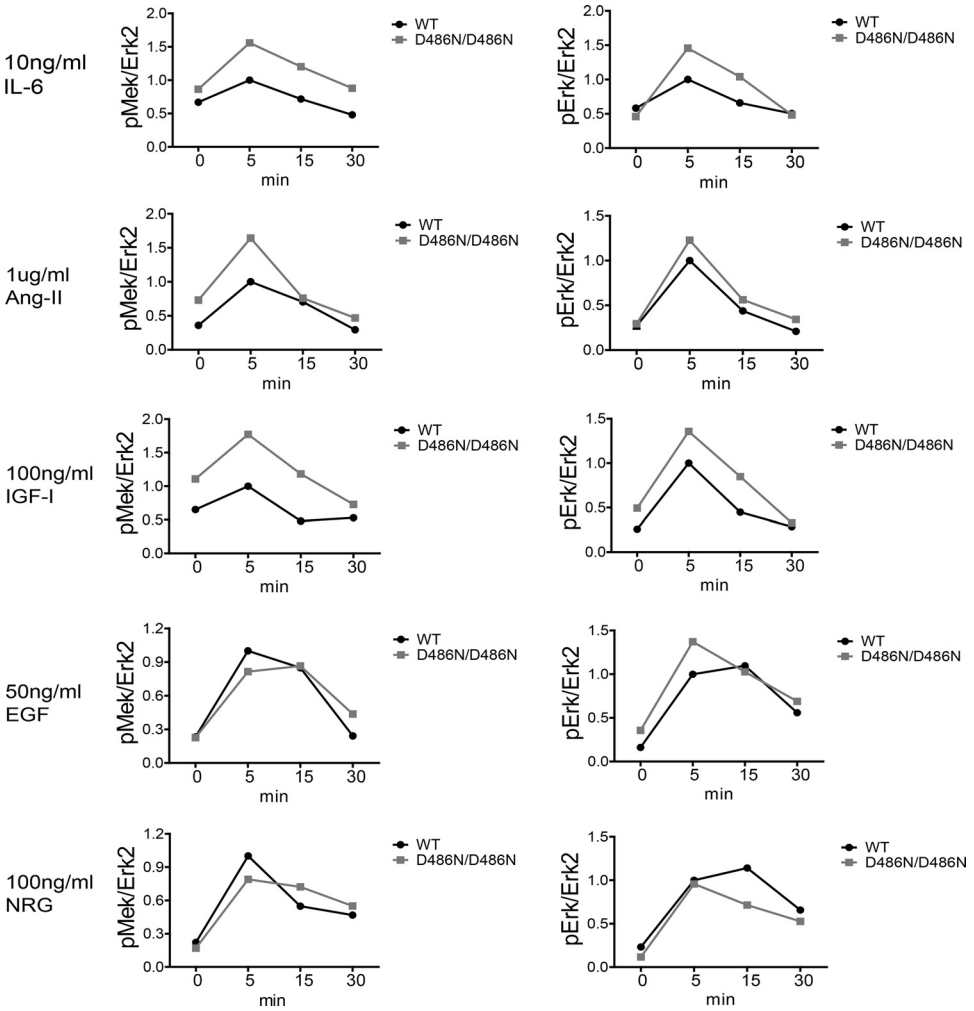

FIG 5 Mek/Erk activation in WT and D486N/D486N neonatal cardiomyocytes. Cardiomyocytes prepared from neonatal WT and D486N/D486N mice were starved for 24 h and then stimulated for the indicated times with different agonists, as indicated. Mek/Erk activation ($n = 2$) was analyzed by immunoblotting with specific antibodies and quantified by using Odyssey software.

D486N/D486N mice did not develop splenomegaly (Fig. 3A), nor did they show overt hematological defects (Fig. 3B and C).

Raf1^{D486N} expression increases Mek/Erk activation in response to multiple stimuli. NS-associated *RAF1* mutations include kinase-activating mutations (e.g., S257L and L613V) and mutations with impaired kinase activity (e.g., D486N and T491I/R) (31, 36). To begin to investigate why kinase-impaired and -activated RAF1 mutants cause similar phenotypes, we assessed Mek and Erk activation in mouse embryonic fibroblasts (MEFs) prepared from heterozygous and homozygous *Raf1^{D486N}* embryos and stimulated with various agonists. As reported previously (54), Raf1^{L613V}-expressing cells showed enhanced Mek/Erk activation in response to agonists for receptor tyrosine kinases (RTKs), cytokine receptors, and G-protein-coupled receptors (GPCRs). Notably, in D486N/+ MEFs, Raf1 protein levels were only ~60% of WT levels, a finding consistent with previous work showing that Raf1 kinase activity is required to prevent the ubiquitin-mediated proteolysis of Raf1 (27). Nevertheless, D486N/+ MEFs showed sustained Mek and Erk activation in response to EGF (Fig. 4A) and PDGF (data not shown) stimulation. D486N/D486N MEFs had only ~30% of WT Raf1 levels but showed enhanced and sustained Mek and Erk activation (Fig. 4A). Mek and Erk activation was also enhanced in D486N/D486N neonatal cardiomyocytes stimulated with cytokine receptor (IL-6), GPCR (Ang-II), or RTK (IGF-I, EGF, and NRG) ligands (Fig. 4B and 5), providing a potential explanation for cardiac hypertrophy in D486N/D486N mice (Fig. 2). Cardiac fibroblasts have also been implicated in hypertrophy pathogenesis (43, 48), and compared with their WT counterparts, neonatal D486N/D486N cardiac fibroblasts showed enhanced Mek/Erk activation in response to multiple agonists (Fig. 4C and 6).

Quantitative differences in effects of NS-associated Raf1 D486N and L613V mutants on Mek/Erk activation. Kinase-activating (e.g., L613V) and kinase-impaired (e.g., D486N) *RAF1* mutants cause NS, but HCM is highly associated only with the former (11, 31, 36). Remarkably, our *Raf1^{L613V}* (L613V/+) (54) and *Raf1^{D486N}* mouse models showed analogous genotype-dependent phenotypic differences (Table 2). L613V/+ mice exhibit HCM that progresses to chamber dilatation (54). In contrast, D486N/+ mice had no obvious cardiac phenotype, but the doubling of the

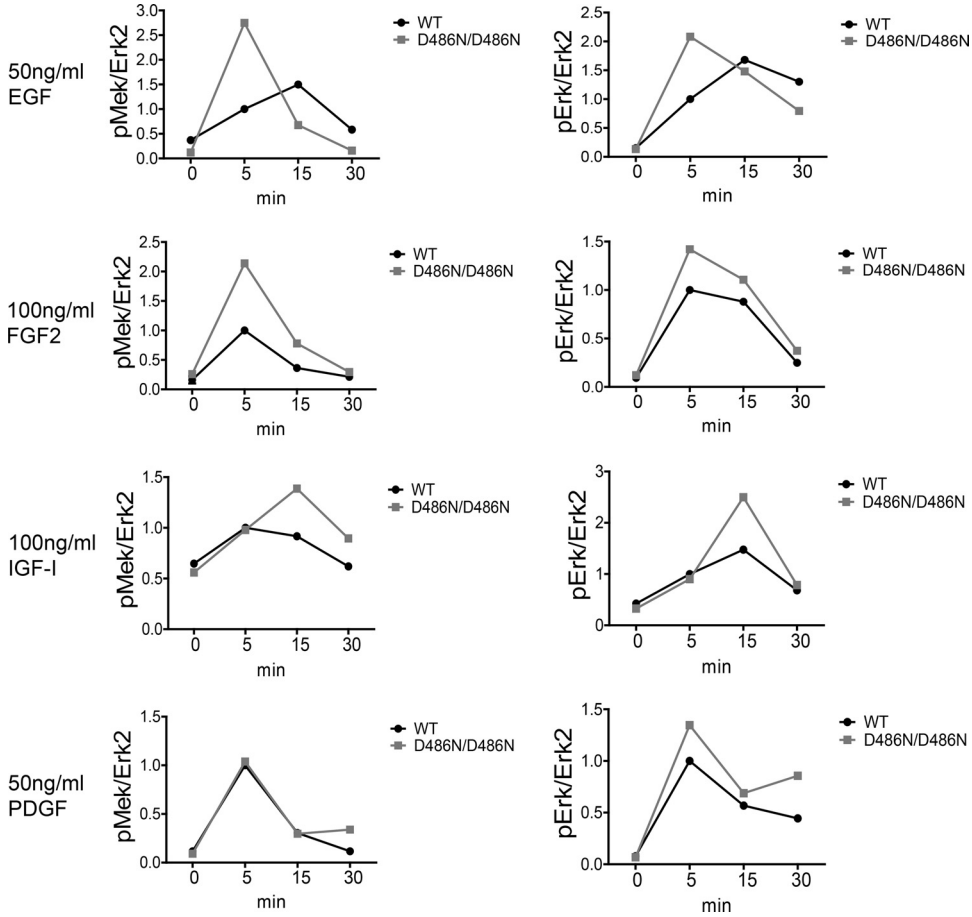

FIG 6 Mek/Erk activation in WT and D486N/D486N neonatal cardiac fibroblasts. Cardiac fibroblasts prepared from neonatal WT and D486N/D486N mice were starved for 24 h and then stimulated for the indicated times with different agonists, as indicated. Mek/Erk activation ($n = 2$) was analyzed by immunoblotting with specific antibodies and quantified by using Odyssey software.

TABLE 2 Comparison of cardiac phenotypes in D486N/D486N and L613V/+ mice[a]

Parameter	Mean value for group ± SEM		
	WT ($n = 20$)	D486N/D486N ($n = 12$)	L613V/+ ($n = 11$)
LVPWd (mm)	0.73 ± 0.01	0.87 ± 0.03***	0.81 ± 0.02*
LVIDd (mm)	4.08 ± 0.04	4.03 ± 0.08##	4.47 ± 0.14**
LVIDs (mm)	2.87 ± 0.06	2.59 ± 0.09**#	2.96 ± 0.12
SV (μl)	41.4 ± 0.9	47.9 ± 3.4**#	57.5 ± 3.3***
CO (ml/min)	20.3 ± 0.5	23.8 ± 1.2**#	27.8 ± 2.1***
FS (%)	29.6 ± 0.9	35.3 ± 1.6**	34.0 ± 1.0*
EF (%)	56.8 ± 1.4	64.3 ± 2.2*	62.9 ± 1.5*
dP/dt max (mm Hg/s)	10,390 ± 347	10,707 ± 690#	12,486 ± 414**

[a] Shown are echocardiographic and invasive hemodynamic parameters of 4-month-old WT ($n = 12$), D486N/D486N ($n = 12$), and L613V/+ ($n = 11$) hearts. LVPWD, left ventricular diastolic posterior wall thickness; LVIDs, left ventricular internal end-systolic dimension; LVIDd, left ventricular internal end-diastolic dimension; SV, stroke volume; FS, fractional shortening; CO, cardiac output; EF, ejection fraction; dP/dt, change of pressure over time. Phenotypic data for L613V/+ mice are derived from our previous publication (54). *, $P < 0.05$; **, $P < 0.01$; ***, $P < 0.001$ (WT versus L613V/+ or WT versus D486N/D486N mice); #, $P < 0.05$; ##, $P < 0.01$ (D486N/D486N versus L613V/+ mice) (determined by a Bonferroni posttest when ANOVA was significant).

dosage of this kinase-defective *Raf1* allele (e.g., in D486N/D486N mice) resulted in concentric cardiac hypertrophy with a decreased left ventricular end-systolic dimension and a normal end-diastolic dimension (Fig. 2).

We asked whether these phenotypic differences correlated with differential effects on Mek/Erk activation. Indeed, $Raf1^{L613V}$ caused a dramatic increase of the magnitude of EGF-evoked Mek/Erk activation in primary MEFs, whereas $Raf1^{D486N}$ resulted mainly in sustained Mek/Erk activation (Fig. 7A). More importantly, Mek activation was enhanced only slightly in hearts from D486N/D486N mice, whereas L613V/+ hearts showed a more profound increase in Mek activation (Fig. 7B). Although $Raf1^{L613V}$ and $Raf1^{D486N}$ enhanced Mek/Erk activation in neonatal cardiomyocytes and cardiac fibroblasts, their effects on the responses to various stimuli differed (Fig. 8). In some cases (e.g., IL-6 and FGF2), $Raf1^{L613V}$ and $Raf1^{D486N}$ had similar effects on pathway activation, but in many others (e.g., Ang-II, NRG, EGF, and PDGF), $Raf1^{L613V}$ had a much stronger effect. Both the magnitude and the duration of Mek/Erk activation were affected differentially by $Raf1^{L613V}$ and $Raf1^{D486N}$. Such differences likely reflect important, if sometimes subtle, differences in the regulation of the RAS/ERK pathway in response to distinct agonists and in different cell types. However, given that Mek inhibitor treatment

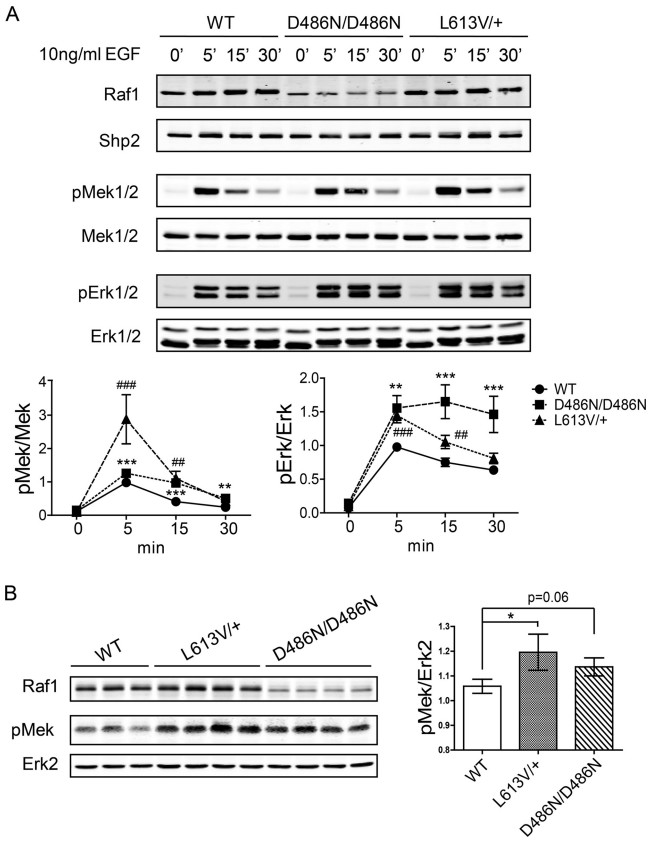

FIG 7 NS-associated Raf1 mutants differentially activate Mek/Erk. (A) Primary WT, D486N/D486N, and L613V/+ MEFs were starved for 16 h and then stimulated with EGF, as indicated. Cell lysates were immunoblotted with the indicated antibodies (p, phospho). The top panel shows a representative blot; the quantification of blots from all experiments ($n = 4$) is shown below. **, $P < 0.01$; ***, $P < 0.001$ (D486N/D486N versus WT mice). ##, $P < 0.01$; ###, $P < 0.001$ (L613V/+ versus WT mice) (determined by a Bonferroni posttest when ANOVA was significant). (B) Mek activation in heart tissues. Lysates from WT ($n = 7$), L613V/+ ($n = 4$), and D486N/D486N ($n = 4$) hearts were analyzed by immunoblotting with anti-pMek antibodies, with Erk2 as a loading control. Representative samples for each genotype are shown on the left. Each lane represents an individual animal. The quantification of all samples is shown on the right. *, $P < 0.05$ (determined by a 2-tailed Student t test).

reverses HCM in L613V/+ mice (54), these data are consistent with the idea that the ability of kinase-activating Raf1 mutants to more profoundly enhance Mek/Erk pathway activation underlies their distinct phenotypic effects (see Discussion).

Kinase-impaired Raf1 mutants enhance Mek/Erk activation by promoting heterodimerization with Braf. To study the biochemical properties of RAF1 mutants in a more biochemically tractable cell system while avoiding the marked overexpression seen in transient-transfection experiments, we generated stable mammalian Flp-In T-REx 293 (T-REx 293) cell lines. Such cells allow the tetracycline-inducible expression of Flag-tagged WT and mutant RAF1 from the same genomic locus at levels comparable to those of endogenous RAF1. As in primary MEFs, cardiomyocytes, and cardiac fibroblasts, the expression of $RAF1^{D486N}$ in T-REx 293 cells resulted in increased MEK/ERK activation, compared with the effects of $RAF1^{WT}$ expression (Fig. 9A).

Transient-transfection studies have shown that RAF1 can form heterodimers with BRAF, that RAF1/BRAF heterodimers have increased kinase activity compared with those of the respective homodimers or monomers, and that a single kinase-competent RAF isoform can confer a high level of catalytic activity to the heterodimer (12, 15, 40, 52). These findings suggested that $RAF1^{D486N}$ might enhance MEK/ERK activation by promoting heterodimer formation. To test this possibility, we immunoprecipitated Flag-tagged RAF1 from induced T-REx 293 cell lysates and subjected the immunoprecipitates to immunoblotting with anti-BRAF antibodies. Following EGF stimulation, low levels of RAF1/BRAF heterodimers were found in WT RAF1-expressing T-REx 293 cell lysates. In contrast, heterodimerization was enhanced dramatically in $RAF1^{D486N}$-expressing cells, even though, as in MEFs, $RAF1^{D486N}$ accumulated to levels considerably lower than those of WT RAF1 (Fig. 9A). The increased heterodimerization was not due to defective negative feedback (7), as heterodimerization was increased even when ERK activation was blocked by MEK inhibitor treatment (Fig. 9B). These results were confirmed by using primary D486N/+ and D486N/D486N MEFs, despite their markedly lower expression levels of $Raf1^{D486N}$ (Fig. 9C). Furthermore, the enhanced ability to form RAF1/BRAF heterodimers was a common feature of kinase-impaired, NS-associated RAF1 mutants: the T491I and T491R kinase domain mutants also showed enhanced heterodimerization and increased and sustained MEK/ERK activation in EGF-stimulated T-REx 293 cells (Fig. 10).

Heterodimerization with BRAF is required for $RAF1^{D486N}$ to enhance MEK/ERK activation. We next asked whether heterodimerization with BRAF is required for enhanced MEK/ERK activation in these cells. Indeed, infection of T-REx 293 cells expressing $RAF1^{D486N}$ with a lentivirus expressing *BRAF* shRNA abolished MEK/ERK hyperactivation in these cells (Fig. 11A). Similar experiments were performed on primary D486N/D486N MEFs. Again, Mek activation and Raf1/Braf heterodimer levels were reduced significantly in *Braf* knockdown cells (Fig. 11B and C). Surprisingly, Erk activation was not affected, although this could reflect a significant upregulation of Erk1 protein levels in *Braf* knockdown MEFs (Fig. 11B).

Mammals express three RAF family members, RAF1, BRAF, and ARAF (25), all of which share MEK1/2 as the substrate. Coimmunoprecipitation experiments using lysates from D486N/D486N MEFs showed that Araf was also present in Raf1 immunoprecipitates (Fig. 11D). However, the *Araf* knockdown did not reduce Mek activation significantly in these cells, compared with the marked effects of *Braf* depletion. The *Braf* knockdown did cause enhanced Araf/Raf1 heterodimerization, which led us to test whether heterodimerization with Araf helps to explain the persistent Mek/Erk activation in Braf knockdown cells. As expected, the combined depletion of *Araf* and *Braf* in these cells further impaired Mek/Erk activation. Taken together, these results suggest that, at least in MEFs, $Raf1^{D486N}$ enhances Mek/Erk activation primarily by promoting heterodimerization with Braf but raise the possibility that Araf/Raf1 heterodimers might contribute to the effects of $Raf1^{D486N}$ in other cell types.

Although these experiments showed that Braf and, to a lesser extent, Araf are necessary for the effects of $Raf1^{D486N}$ and that these effects correlate with the ability of this mutant to increase heterodimerization, they did not establish a causal relationship between heterodimerization and Mek/Erk hyperactivation. Previous structural studies of *Drosophila melanogaster* Raf (35) showed

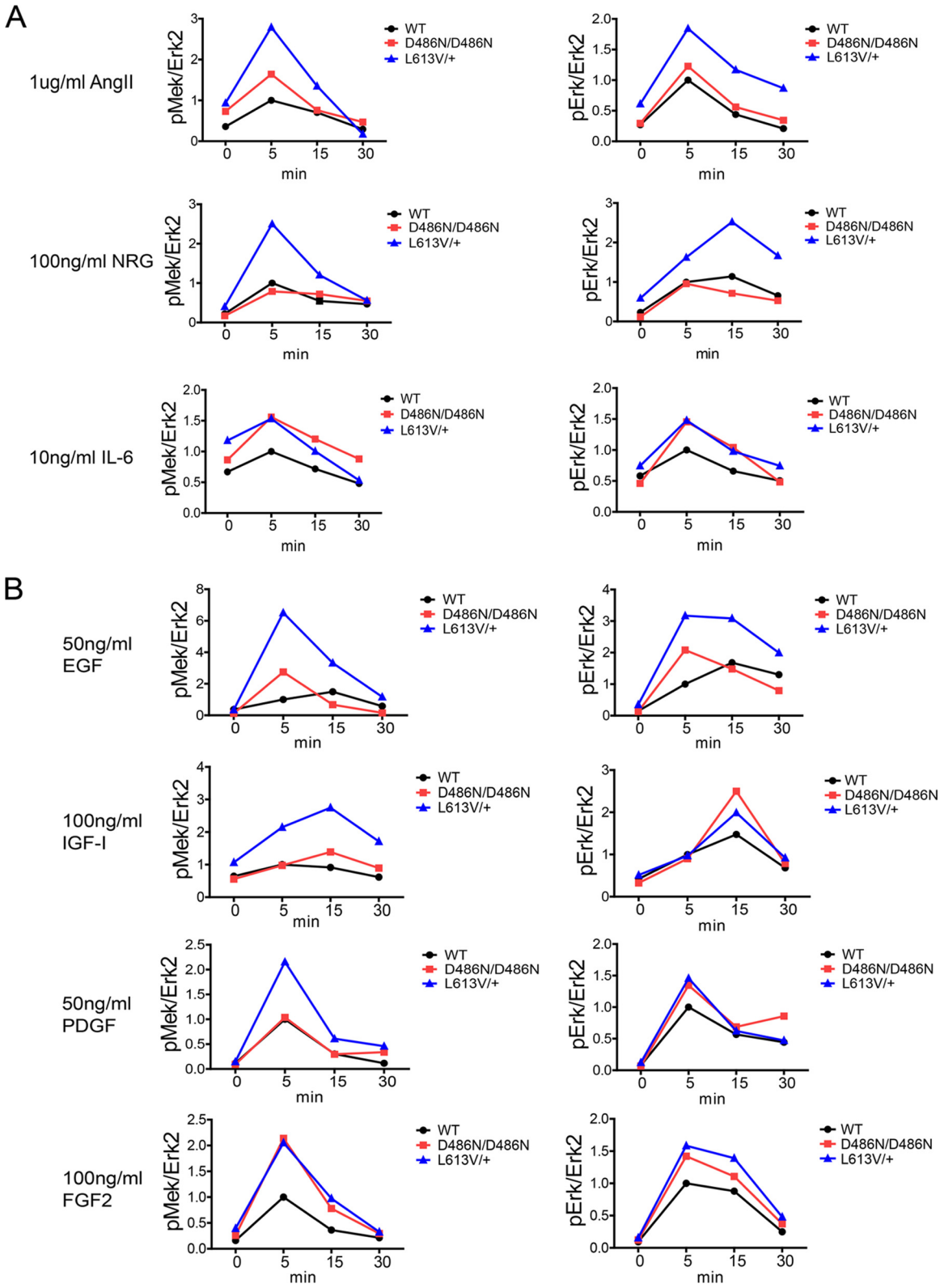

FIG 8 Severity of the cardiac phenotype in D486N/D486N and L613V/+ mice correlates with Mek/Erk activation. Shown is the quantification of Mek/Erk activation from immunoblots ($n = 2$) of cardiomyocytes (A) and cardiac fibroblasts (B). Lysates from neonatal WT and D486N/D486N or WT and L613V/+ cells were starved for 24 h and then stimulated as indicated. Values indicate fold changes in Mek/Erk activity (assessed by immunoblotting with phospho-specific antibodies) in D486N/D486N or L613V/+ cells, compared with the corresponding WT control at 5 min poststimulation.

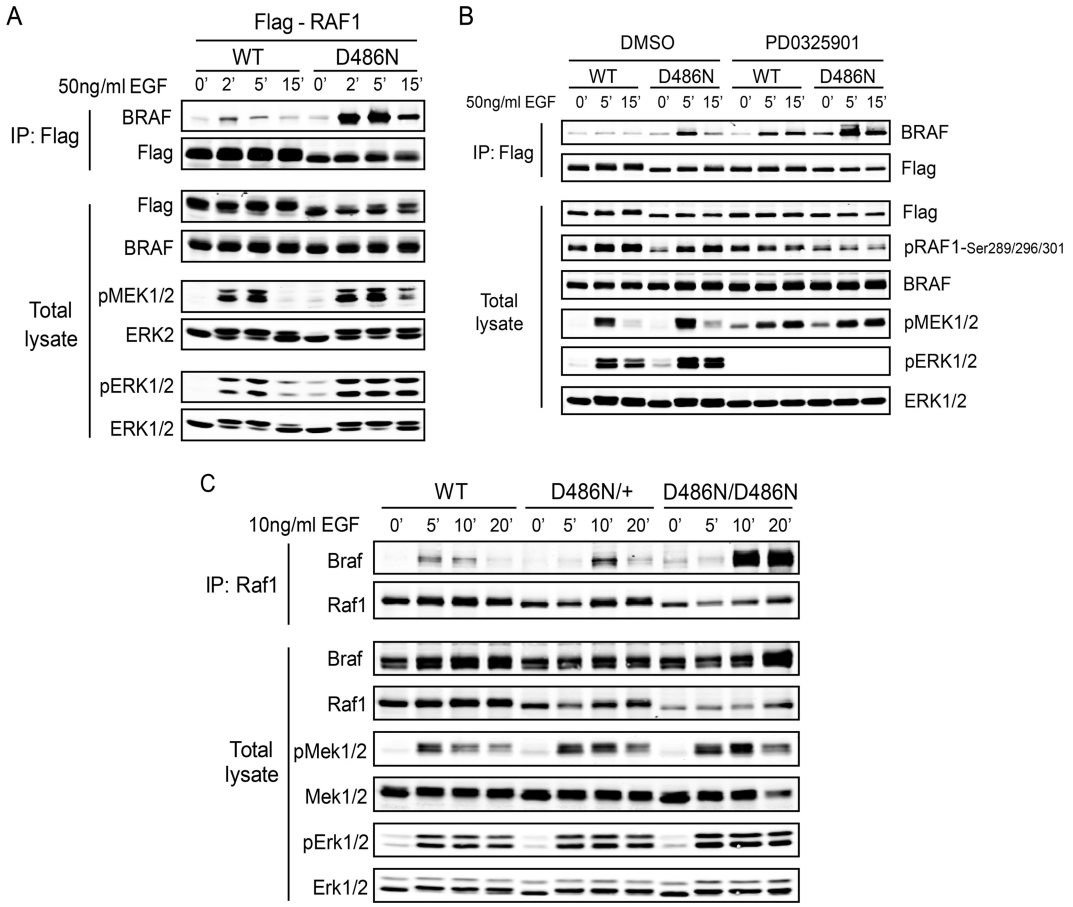

FIG 9 RAF1^{D486N} forms more heterodimers with BRAF. (A) T-REx 293 cell lines expressing Flag-tagged human WT or D486N mutant RAF1 were incubated with 1 μg/ml tetracycline for 20 h in serum-free medium and then stimulated with EGF for the indicated times. Heterodimers were detected by immunoprecipitation (IP) with an anti-Flag antibody, followed by blotting for endogenous BRAF. MEK and ERK activation in the same lysates was assessed by immunoblotting. (B) T-REx 293 cell lines expressing Flag-tagged human WT RAF1 or the D486N mutant were incubated with 1 μg/ml tetracycline for 20 h in serum-free medium and then treated with 10 μM PD0325901 for 1 h before stimulation with EGF for the indicated times. Heterodimers were detected by immunoprecipitation with an anti-Flag antibody, followed by blotting for BRAF. Total cell lysates from the same experiment were immunoblotted with the indicated antibodies. (C) Primary MEFs from WT, D486N/+, and D486N/D486N mice were starved for 16 h and then stimulated with EGF, as indicated. Endogenous heterodimers were detected by immunoprecipitation with an anti-RAF1 antibody, followed by blotting for Braf. Mek and Erk activation in the same lysates was assessed by immunoblotting.

that Arg481 (Arg401 in RAF1 and Arg509 in BRAF) is at the center of a side-to-side RAF dimer interface and participates directly in these interactions (Fig. 12A). As in *Drosophila* Raf, the introduction of the R401H mutation into WT RAF1 or RAF1^{D486N} abolished RAF1/BRAF heterodimerization (Fig. 12B). Moreover, the compound R401H/D486N mutant no longer enhanced EGF-evoked MEK/ERK activation (Fig. 12C). Similar results were obtained when we tested another mutation (F408A) within the dimer interface (Fig. 12A and D). Furthermore, the reexpression of Myc-tagged WT Braf in *Braf* knockdown D486N/D486N MEFs restored Mek and Erk activation, whereas Braf^{R509H} could not (Fig. 12E).

Finally, to test unambiguously the effects of dimerization *per se* (as opposed to other, unanticipated structural consequences of dimer interface mutants), we asked if forced heterodimerization could restore the ability of RAF1$^{R401H/D486N}$ to promote MEK/ERK activation. We fused Flag-RAF1$^{R401H/D486N}$, which cannot form heterodimers with BRAF, to FKBP, while FRB was fused to BRAF (Fig. 13A). Upon cotransfection, these two proteins can heterodimerize only upon the addition of a rapamycin analog (A/C heterodimerizer). Remarkably, MEK activation and ERK activation were restored upon the addition of the A/C heterodimerizer (Fig. 13B); importantly, the heterodimerizer itself had no effect (Fig. 13C). Taken together, these results show that heterodimerization with BRAF is necessary and sufficient for the NS-associated RAF1^{D486N} mutant to enhance MEK/ERK activation.

Surprisingly, we noticed that the kinase-activating mutant RAF1^{L613V} also formed more RAF1/BRAF heterodimers in response to growth factor stimulation (Fig. 12B and 14A), and as for the kinase-defective *Raf1* alleles, the knockdown of *Braf* in primary MEFs expressing *Raf1*^{L613V} significantly reduced Mek activation in these cells (data not shown). Moreover, the double mutant L613V and dimer mutant (R401H) abolished RAF1/BRAF heterodimerization and no longer caused enhanced MEK/ERK activation (Fig. 12B and 14B). These data provide an explanation for the ability of this class of kinase-activated alleles to promote MEK/ERK hyperactivation.

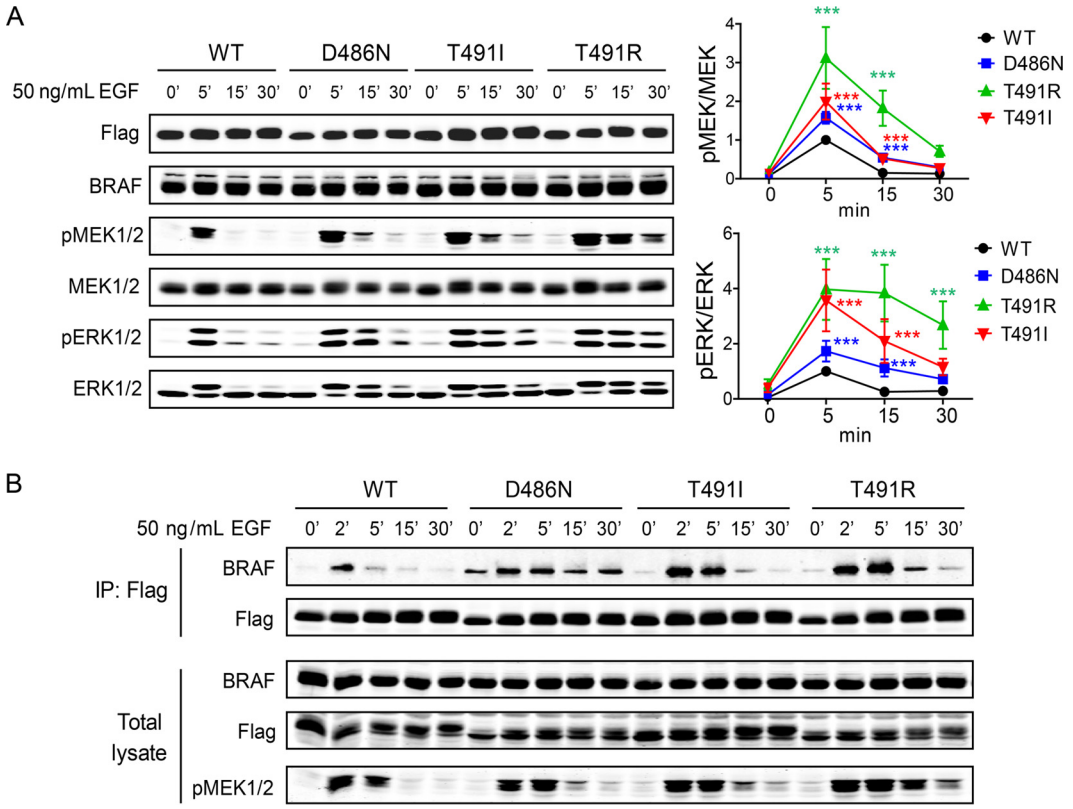

FIG 10 Kinase-impaired RAF1 mutants associated with NS enhance MEK/ERK activation and form more RAF1/BRAF heterodimers. (A) T-REx 293 cell lines expressing Flag-tagged human WT or D486N, T491I, or T491R mutant RAF1 were incubated with 1 μg/ml tetracycline for 20 h in serum-free medium and then stimulated with EGF. Cell lysates from a representative experiment were subjected to immunoblotting with the indicated antibodies. The quantification of blots from all experiments ($n = 4$) is shown on the right. ***, $P < 0.001$ (WT versus the D486N mutant, WT versus the T491I mutant, and WT versus the T491R mutant) (determined by a Bonferroni posttest when ANOVA was significant). (B) T-REx 293 cell lines expressing Flag-tagged human WT RAF1 or the indicated mutants were incubated with 1 μg/ml tetracycline for 20 h in serum-free medium and then stimulated with EGF. Heterodimers were detected by immunoprecipitation with an anti-Flag antibody, followed by immunoblotting for BRAF. The same lysates were immunoblotted with the indicated antibodies.

DISCUSSION

We generated and analyzed a knock-in mouse model for the NS-associated, kinase-impaired *Raf1*^{D486N} mutation. Unlike the kinase-activating mutation *Raf1*^{L613V} (54), which causes most major features of NS, including proportional short stature, facial dysmorphia, hematological defects, and HCM, *Raf1*^{D486N} heterozygosity results in only a mild growth defect in female mice. *Raf1*^{D486N} homozygous mice (on a 129Sv × C57BL/6 mixed background) exhibit concentric cardiac hypertrophy (but not HCM) and an incompletely penetrant severe growth defect that is accompanied by facial dysmorphia, failure to thrive, and early death. A detailed analysis of the mechanism underlying the effects of this *Raf1* allele as well as other kinase-defective RAF1 mutants indicated that they paradoxically hyperactivate the RAS/ERK pathway by promoting heterodimerization with BRAF and, to a lesser extent, ARAF. Finally, we unexpectedly found that Raf1^{L613V}, whose activation mechanism had remained unclear, also promotes increased heterodimer formation. Taken together, these data identify an increased heterodimerization capacity as the common theme in the pathogenesis of *RAF1* mutant-associated NS.

The incompletely penetrant growth/facial dysmorphia/viability phenotype of D486N/D486N mice suggests the existence of a modifier gene(s) that varies between the 129Sv and C57BL/6 strains. Indeed, preliminary mapping studies have identified a 129Sv locus on mouse chromosome 8 that is strongly linked (logarithm of odds [LOD] score of ~15) to the s-D486N/D486N phenotype. Like s-D486N/D486N mice, *Araf*-deficient mice have severe growth defects, neurological abnormalities, and postnatal lethality (34); notably, these phenotypes also are sensitive to the genetic background. The identification of loci that modify Raf1 function could provide important insights into the regulation of Raf-dependent signaling, and it will be interesting to see if the same modifier(s) affects the *Raf1*^{D486N} and *Araf* mutant phenotypes. Primary lung fibroblasts prepared from s- and n-D486N/D486N mice showed comparable Mek/Erk activation (data not shown), suggesting that the putative modifier(s) likely acts downstream of Erk or parallel to the RAS/ERK pathway. Our previous NS mouse models, Shp2^{D61G} (3) and Raf1^{L613V} (54), also showed strain-specific differences in phenotypes. However, different modifiers are likely to be involved, because an increase of the C57BL/6 content causes lethality in these two mouse models. Given the marked genetic heterogeneity of the human population and the differences in penetrances of RASopathy phenotypes within a single affected family, not to mention between unrelated patients with the same mutant allele, our mouse

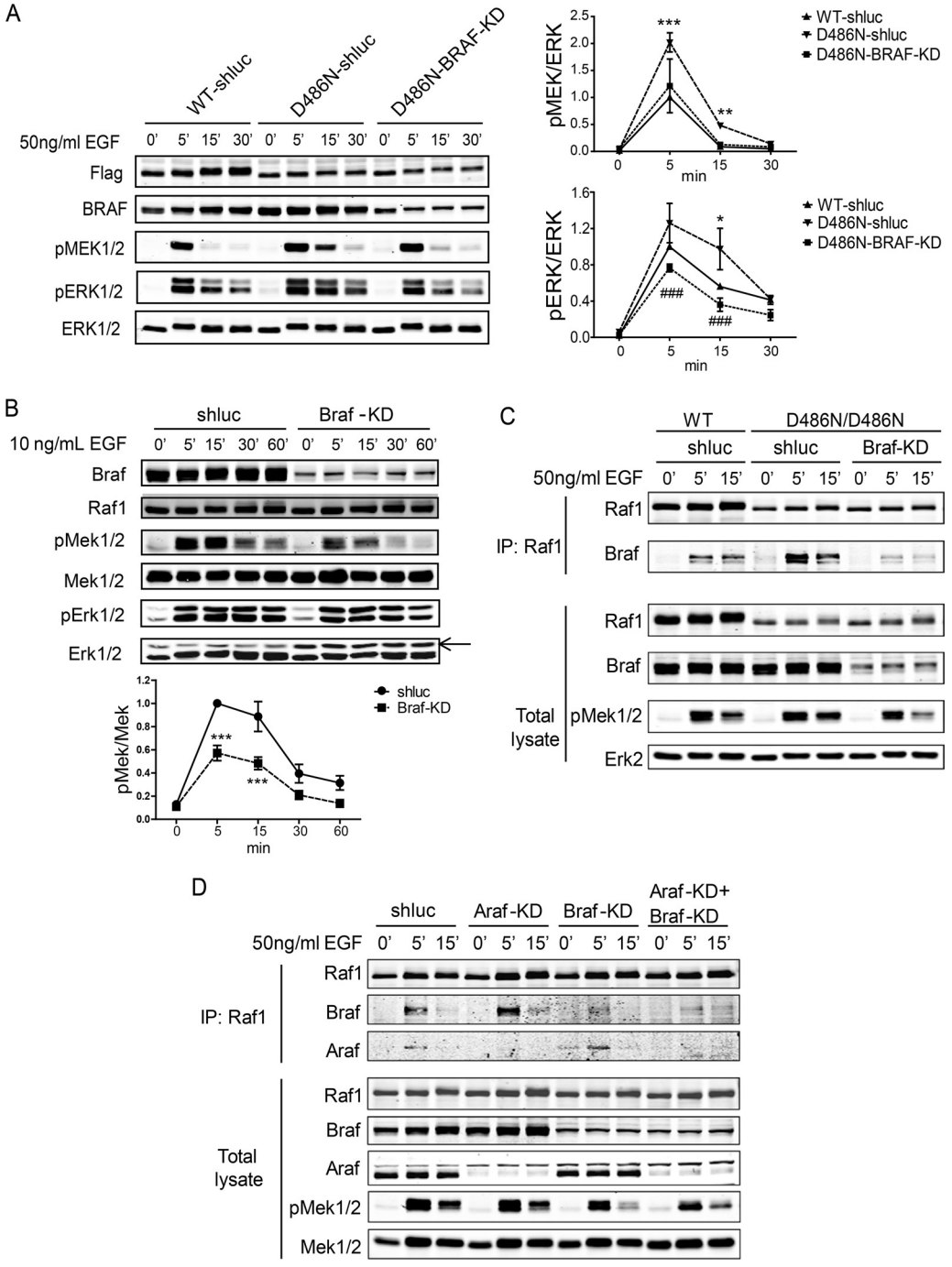

FIG 11 BRAF is required for RAF1^{D486N} to enhance MEK/ERK activation. (A) T-REx 293 cell lines expressing Flag-tagged human WT or D486N mutant RAF1 were infected with a lentivirus expressing *BRAF* shRNA (BRAF-KD) or a control (luciferase) shRNA (shluc). At 48 h after puromycin selection, cells were incubated with 1 μg/ml tetracycline for 20 h in serum-free medium and then stimulated with EGF. Cell lysates were immunoblotted with the indicated antibodies. A representative experiment is shown on the left, and blots from all experiments ($n = 3$) are quantified on the right. *, $P < 0.05$; **, $P < 0.01$; **, $P < 0.001$ (WT-shluc versus D486N-shluc). ###, $P < 0.001$ (D486N-shluc versus D486N-BRAF-KD) (determined by a Bonferroni posttest when ANOVA was significant). (B) Primary MEFs from D486N/D486N mice were infected with a lentivirus expressing *Braf* shRNA (Braf-KD) or a control shRNA (shluc). Cell lysates were immunoblotted with the indicated antibodies. A representative blot is shown at the top (the arrow indicates the position of Erk1). The quantification of blots from all experiments ($n = 4$) for Mek activation is shown at the bottom. ***, $P < 0.001$ (determined by a Bonferroni posttest when ANOVA was significant). (C) Primary WT and D486N/D486N MEFs were infected with a lentivirus expressing *Braf* shRNA (Braf-KD) or a control shRNA (shluc). Heterodimers were detected by immunoprecipitation with an anti-RAF1 antibody, followed by immunoblotting for BRAF. Total cell lysates were immunoblotted with the indicated antibodies. (D) Primary D486N/D486N MEFs were infected with lentiviruses expressing shRNAs against *Braf* (Braf-KD) and/or *Araf* (Araf-KD) or a control shRNA (shluc). Heterodimers were detected by immunoprecipitations with an anti-RAF1 antibody, followed by blotting for Braf or Araf. Total cell lysates were also immunoblotted with the indicated antibodies.

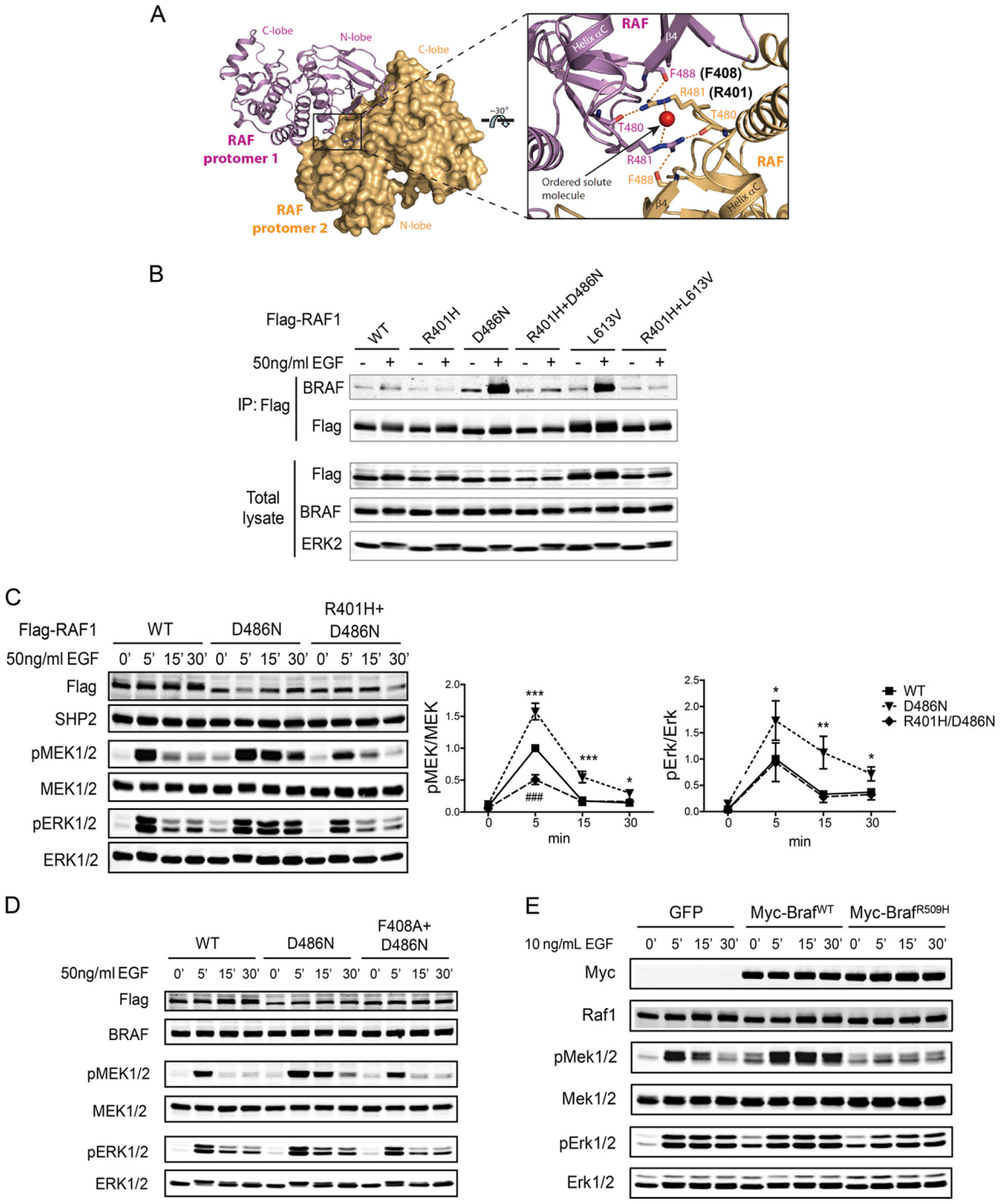

FIG 12 Heterodimerization with BRAF is required for the RAF1^{D486N} mutant to enhance MEK/ERK activation. (A) Side-to-side dimer interface in *Drosophila* Raf (expanded [right] portion adapted from reference 35 with permission). One protomer is displayed as a surface representation in orange, while the other is shown as a ribbon representation in violet. The inset shows a close-up of hydrogen-bonding interactions involving R481 and F488 (R401 and F408 in human RAF1). (B) T-REx 293 cell lines expressing Flag-tagged human WT RAF1 or the indicated mutants were incubated with 1 μg/ml tetracycline for 20 h in serum-free medium and then either left unstimulated (−) or stimulated with EGF for 5 min (+). Heterodimers were detected by immunoprecipitation with an anti-Flag antibody, followed by immunoblotting with anti-BRAF antibodies. Total cell lysates were also immunoblotted with the indicated antibodies. (C) T-REx 293 cell lines expressing Flag-tagged human WT RAF1 or the indicated mutants were incubated with 1 μg/ml tetracycline for 20 h in serum-free medium and then stimulated with EGF for the times indicated. Cell lysates were immunoblotted with the indicated antibodies. A representative immunoblot is shown, and the quantification of the blots from all experiments ($n = 4$) is shown at the bottom. *, $P < 0.05$; **, $P < 0.01$; ***, $P < 0.001$ (WT versus D486N). ###, $P < 0.001$ (R401H/D486N versus WT) (determined by a Bonferroni posttest when ANOVA was significant). (D) T-REx 293 cell lines expressing Flag-tagged human WT RAF1 or the D486N and/or F408A mutant were incubated with 1 μg/ml tetracycline for 20 h in serum-free medium and then stimulated with EGF for the times indicated. Cell lysates were immunoblotted with the indicated antibodies. (E) Immortalized D486N/D486N MEFs were infected with a lentivirus expressing *Braf* shRNA. At 72 h after puromycin selection, cells were infected with MCSV-based retroviruses expressing GFP alone or GFP plus Myc-BRAF^{WT} or Myc-BRAF^{R509H}. GFP-positive cells, obtained by FACS, were serum starved for 16 h and then were stimulated with EGF. Cell lysates were immunoblotted with the indicated antibodies.

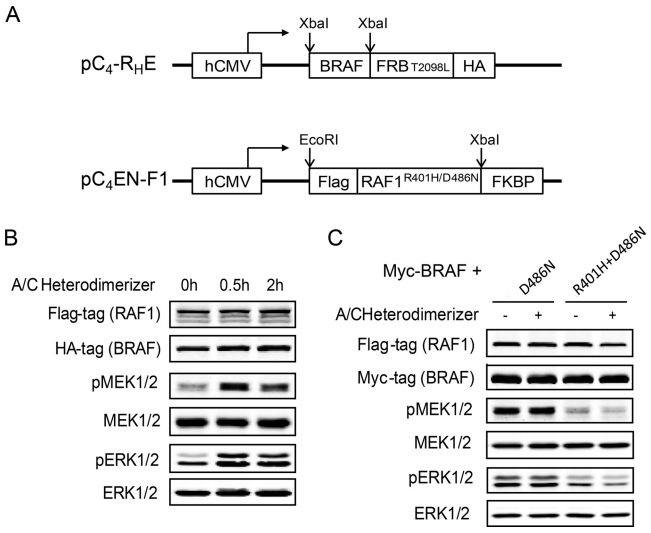

FIG 13 Induced RAF1/BRAF heterodimerization restores the activity of the RAF1$^{R401H/D486N}$ mutant to enhance MEK/ERK activation. (A) *RAF1$^{R401H/D486N}$* and *BRAF* coding sequences were subcloned into FKBP and PRB expression vectors, respectively, as shown. (B) T-REx 293 cells were cotransfected with Flag-RAF1$^{R401H/D486N}$-FKBP and BRAF-FRB-HA expression plasmids for 24 h and then left untreated (0 h) or treated with the A/C heterodimerizer (500 nM) for the indicated times. Cell lysates were immunoblotted with the indicated antibodies. (C) T-REx 293 host cells were cotransfected with *Flag-RAF1^{D486N}* or *Flag-RAF1$^{R401H/D486N}$* and *Myc-BRAF* expression plasmids and 24 h later were left untreated (−) or treated with the A/C heterodimerizer (500 nM) (+) for 30 min. Cell lysates were immunoblotted with the indicated antibodies.

models provide excellent opportunities to investigate the relative effects of RASopathy mutations and genetic backgrounds.

Kinase-activating *RAF1* mutants are strongly associated with HCM in human NS patients, a phenotype reproduced by our *Raf1^{L613V}* mouse model (54). Similarly, D486N/+ mice, like NS patients with kinase-impaired *RAF1* mutations, do not exhibit HCM. Notably, *Raf1^{D486N}* homozygosity (which is not seen in humans) results in concentric cardiac hypertrophy that does not progress to heart failure within 1 year of observation (Fig. 2 and data not shown), unlike the eccentric cardiac hypertrophy seen in L613V/+ mice (54). Biochemical analyses revealed that, in contrast to initial reports based on transient-transfection experiments (31), the expression of kinase-impaired Raf1^{D486N} at normal (endogenous) levels causes sustained and/or enhanced Mek/Erk activation in multiple cell types in response to a variety of stimuli. In order to transmit signals downstream, RAF proteins must assemble into multiprotein complexes (25). Presumably, the substantial overexpression that occurs in transiently transfected cells results in artifactual dominant negative effects of kinase-deficient RAF1 mutants that are not seen when these proteins are expressed at appropriate, endogenous levels. Importantly, however, Raf1^{D486N} is less potent than Raf1^{L613V} in enhancing Mek/Erk activation in response to most stimuli, in both cardiomyocytes and cardiac fibroblasts (Fig. 8). Furthermore, Raf1^{L613V} generally increases the magnitude of Mek/Erk activation, whereas Raf1^{D486N} most often prolongs the signal duration. Given our previous finding that HCM can be prevented or reversed by MEK inhibitor treatment of Raf1$^{L613V/+}$ mice, these data strongly suggest that differences in the abilities of the D486N and L613V mutants (and, by inference, between kinase-impaired and kinase-activated RAF1 in general) to promote Mek/Erk activation in the heart explain their distinct cardiac phenotypes. If so, then agonists that show differential effects on Mek/Erk pathway activation in *Raf1$^{L613V/+}$* and *Raf1$^{D486N/D486N}$* cardiomyocytes (e.g., Ang-II and NRG but not IL-6) and/or cardiac fibroblasts (e.g., EGF, IGF, and PDGF but not FGF2) might be particularly important for cardiac hypertrophy in NS. Raf1^{D486N} accumulates to much lower levels than Raf1^{L613V}, consistent with a previous report that kinase activity is required to prevent Raf1 degradation (27). Consequently, we cannot ascertain whether lower levels of the Raf1^{D486N} protein or its lower level of kinase activity accounts for the decreased Mek/Erk hyperactivation seen in D486N/D486N compared with that seen in L613V/+ mice (also see below).

The carboxyl oxygen of the highly conserved aspartic acid 486 (the "D" of the DFG motif) plays a critical role in chelating Mg^{2+} and stabilizing ATP binding in the active site of protein kinases (17). The mutation of this residue to alanine creates a kinase-inactive protein (27), whereas a mutation to asparagine severely impairs (but does not eliminate) activity (31). All RAF family members require the phosphorylation of key activation loop residues for maximal kinase activation (7, 8), and T491 is one of these residues. As expected, NS-associated mutants affecting T491 also show impaired kinase activity (31).

Our results clearly establish how all such mutants (D486N, T491I, and T491R) enhance downstream MEK/ERK activation. Previous studies showed that RAF1/BRAF heterodimerization occurs during normal growth factor signaling and indicated that heterodimers have an increased catalytic activity compared with that of homodimers or monomers (40). Although some have argued that RAF1 inhibits BRAF activation in a kinase domain-dependent fashion (19), other studies reported that human cancer-associated BRAF mutants with impaired kinase activity promote MEK activation by binding to and *trans*-activating RAF1 (12, 51). Of note, these kinase-impaired mutations alter the activation segment of BRAF, and some (D594G and T599I) are analogous to NS-associated RAF1 mutants (16, 18). Heidorn and colleagues recently reported that mice with a conditional kinase-dead *Braf* (*Braf$^{LSL\text{-}D594A}$*) allele, when combined with oncogenic *Ras* (*Kras^{G12D}*), induced melanomas in mice. In tumor cells from these mice, Braf^{D594A} was bound to Raf1 constitutively (15). By analogy, we suspected that kinase-impaired, NS-associated RAF1 mutants hyperactivated MEK/ERK by promoting heterodimerization with BRAF. Indeed, we found that all of the kinase-impaired RAF1 mutants form more heterodimers with BRAF upon growth factor stimulation (Fig. 10). Furthermore, the level of MEK/ERK hyperactivation depends on the level of RAF1/BRAF heterodimerization, as RAF1^{T491I} and RAF1^{T491R} formed more heterodimers and caused more MEK/ERK activation than did RAF1^{D486N} (Fig. 10).

Several subsequent lines of evidence establish a causal relationship between heterodimerization and MEK/ERK activation. First, the knockdown of *BRAF* in T-REx 293 cells expressing Flag-RAF1^{D486N} reduces MEK/ERK activation. *Braf* knockdown in primary D486N/D486N MEFs also impairs Mek activation, although Erk activation is unaffected (Fig. 11). This difference might be more apparent than real, however, as total Erk1 levels are increased in *Braf* knockdown MEFs (Fig. 11B), suggesting potential compensation during the selection of stable knockdown clones. Such feedback regulation presumably is impaired (or less effective) in T-REx 293 cells. Second, the mutation of either of two key

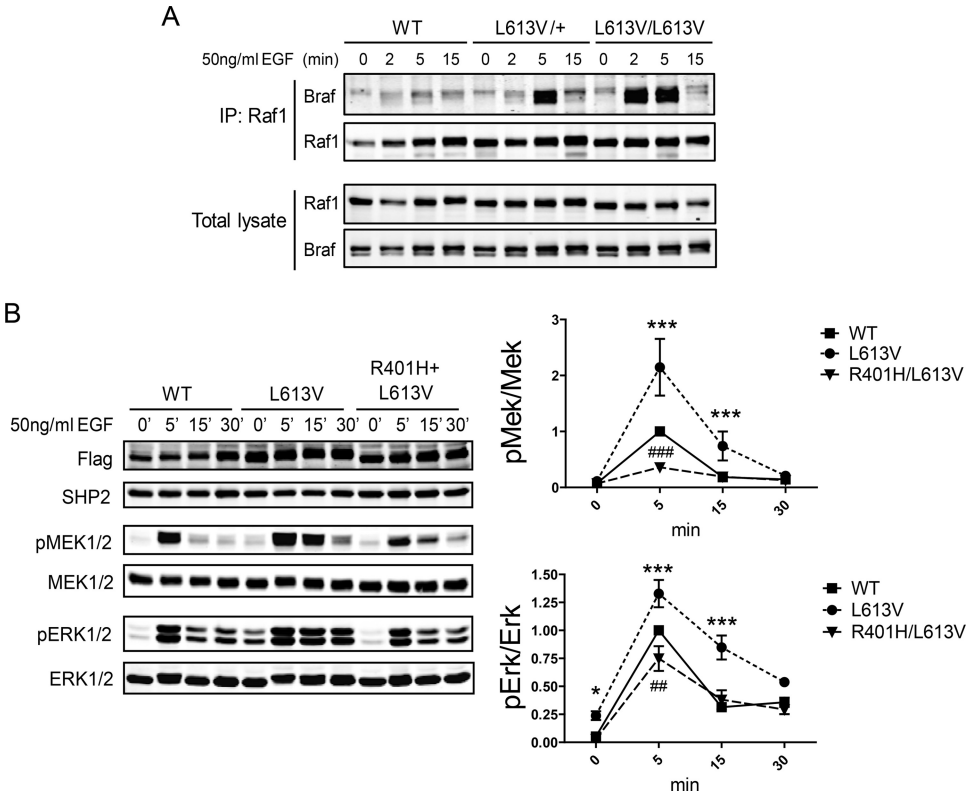

FIG 14 The RAF1^{L613V} mutant enhances MEK/ERK activation via RAF1/BRAF heterodimer formation. (A) Primary WT, L613V/+, and L613V/L613V MEFs were starved for 16 h and then stimulated with EGF for the indicated times. Endogenous heterodimers were detected by immunoprecipitation with an anti-RAF1 antibody, followed by blotting for Braf. Total cell lysates from the same experiments were immunoblotted with the indicated antibodies. (B) T-REx 293 cell lines expressing WT, L613V, or R401H/L613V Flag-RAF1 were incubated with 1 μg/ml tetracycline for 20 h in serum-free medium and then stimulated with EGF for the times indicated. MEK activation and ERK activation were assessed by immunoblotting with the indicated antibodies. A representative immunoblot is shown, and the quantification of the blots from all experiments ($n = 3$) is shown on the right. *, $P < 0.05$; ***, $P < 0.001$ (WT versus the L613V mutant). ##, $P < 0.01$; ###, $P < 0.001$ (R401H/L613V mutant versus the WT) (determined by a Bonferroni posttest when ANOVA was significant).

residues (R401H and F408A) in the dimer interface of the RAF1 kinase domain, as revealed by the crystal structures of BRAF (51) and *Drosophila* Raf (35), abolishes the ability of RAF1^{D486N} to enhance EGF-evoked MEK/ERK activation. Most compellingly, the forced heterodimerization of Raf1$^{D486N/R401H}$ and BRAF by means of an inducible FKBP-FRB interaction system restored the ability of Raf1$^{D486N/R401H}$ to enhance EGF-evoked MEK/ERK hyperactivation (Fig. 12 and 13). The latter result shows unambiguously that Raf1$^{D486N/R401H}$ cannot hyperactivate MEK/ERK solely because it has lost its ability to promote RAF1/BRAF heterodimerization, as opposed to some unanticipated effect of the second-site R401H mutation on the conformation of the D486N mutant. Taken together, our results demonstrate that heterodimerization with BRAF is necessary and sufficient for such mutants to enhance MEK/ERK activation. Although our knockdown studies show that RAF1^{D486N} enhances MEK/ERK activation (at least in MEFs and T-REx 293 cells) mainly through heterodimerization and the transactivation of BRAF, we also find that kinase-defective RAF1 mutants can heterodimerize with ARAF. Consequently, we do not exclude the possibility that RAF1/ARAF heterodimers play an important role in the pathogenesis of NS caused by kinase-defective RAF1 alleles in tissues where ARAF is a major isoform (e.g., the brain).

Another cluster of NS-associated *RAF1* mutations maps to the C terminus (S612 and L613) of RAF1. Like NS-associated CR2 domain mutants, these mutants have increased kinase activity (31), even though S612 and L613 lie distal to the RAF1 kinase domain. Previous studies have not implicated these residues in RAF1 regulation, so it has been unclear how such mutations enhance kinase activity. Moreover, the phosphorylation of Ser259 (an inhibitory binding site for 14-3-3) and phosphorylation of Ser621 (31), a 14-3-3 binding site that promotes RAF1 activation (27), are unaffected in RAF1^{L613V}. We found that RAF1^{L613V} also forms more heterodimers with BRAF upon growth factor stimulation than does WT RAF1. Moreover, superimposing the dimer interface mutant (R401H) on L613V blocked its ability to enhance MEK/ERK activation (Fig. 12B and 14).

These data strongly suggest that RAF1^{L613V} also promotes MEK/ERK hyperactivation via an enhanced BRAF heterodimerization ability. As the kinase domain of RAF1^{L613V} is not altered, and this mutant is expressed at normal levels, unlike kinase-deficient RAF1 alleles, heterodimerization with BRAF presumably results in a greater increase in MEK/ERK activation than that evoked by kinase-impaired RAF1 alleles. The NS-associated CR2 domain mutants RAF1^{S257L} and RAF1^{P261T} (37) (data not shown) also form more heterodimers with BRAF. Taken together, these results argue that the increased ability to heterodimerize with BRAF (and possibly ARAF) represents a general pathogenic mechanism for NS-associated *RAF1* mutations and suggest that

agents that interfere with dimerization might have general utility for the treatment of *RAF1* mutant NS.

ACKNOWLEDGMENTS

We thank Jason Moffat (University of Toronto) for providing lentiviral shRNA vectors.

This work was supported by National Institutes of Health grants HL083273 and R37CA49152 (to B.G.N.); Canadian Institutes of Health Research grants 106526 (to T.A.), 153103 (to P.H.B.), and 111159 (to J.S.); and Heart & Stroke Foundation of Ontario (H&SFO) grant T6485 (to P.H.B.). B.G.N. is a Canada research chair, tier 1, and work in his laboratory is partially supported by the Ontario Ministry of Health and Long Term Care and the Princess Margaret Hospital Foundation. P.H.B. is a career investigator with the H&SFO. X.W. was supported by a Frederick Banting and Charles Best Canada graduate scholarship. K.-H.K. was supported in part by graduate studentships from the Ontario Graduate Scholarship (OGS) in Science and Technology program. S.G. was supported by an MBP Excellence UTF scholarship.

REFERENCES

1. **Aoki Y, Niihori T, Narumi Y, Kure S, Matsubara Y.** 2008. The RAS/MAPK syndromes: novel roles of the RAS pathway in human genetic disorders. Hum. Mutat. **29**:992–1006.
2. **Araki T, et al.** 2009. Noonan syndrome cardiac defects are caused by PTPN11 acting in endocardium to enhance endocardial-mesenchymal transformation. Proc. Natl. Acad. Sci. U. S. A. **106**:4736–4741.
3. **Araki T, et al.** 2004. Mouse model of Noonan syndrome reveals cell type- and gene dosage-dependent effects of Ptpn11 mutation. Nat. Med. **10**:849–857.
4. **Bentires-Alj M, Kontaridis MI, Neel BG.** 2006. Stops along the RAS pathway in human genetic disease. Nat. Med. **12**:283–285.
5. **Chen J, Fujii K, Zhang L, Roberts T, Fu H.** 2001. Raf-1 promotes cell survival by antagonizing apoptosis signal-regulating kinase 1 through a MEK-ERK independent mechanism. Proc. Natl. Acad. Sci. U. S. A. **98**:7783–7788.
6. **Chen PC, et al.** 2010. Activation of multiple signaling pathways causes developmental defects in mice with a Noonan syndrome-associated Sos1 mutation. J. Clin. Invest. **120**:4353–4365.
7. **Chong H, Lee J, Guan KL.** 2001. Positive and negative regulation of Raf kinase activity and function by phosphorylation. EMBO J. **20**:3716–3727.
8. **Chong H, Vikis HG, Guan KL.** 2003. Mechanisms of regulating the Raf kinase family. Cell. Signal. **15**:463–469.
9. **Cirstea IC, et al.** 2010. A restricted spectrum of NRAS mutations causes Noonan syndrome. Nat. Genet. **42**:27–29.
10. **Cordeddu V, et al.** 2009. Mutation of SHOC2 promotes aberrant protein N-myristoylation and causes Noonan-like syndrome with loose anagen hair. Nat. Genet. **41**:1022–1026.
11. **Dhandapany PS, et al.** 2011. Cyclosporine attenuates cardiomyocyte hypertrophy induced by RAF1 mutants in Noonan and LEOPARD syndromes. J. Mol. Cell. Cardiol. **51**:4–15.
12. **Garnett MJ, Rana S, Paterson H, Barford D, Marais R.** 2005. Wild-type and mutant B-RAF activate C-RAF through distinct mechanisms involving heterodimerization. Mol. Cell **20**:963–969.
13. **Giehl K.** 2005. Oncogenic Ras in tumour progression and metastasis. Biol. Chem. **386**:193–205.
14. **Hatzivassiliou G, et al.** 2010. RAF inhibitors prime wild-type RAF to activate the MAPK pathway and enhance growth. Nature **464**:431–435.
15. **Heidorn SJ, et al.** 2010. Kinase-dead BRAF and oncogenic RAS cooperate to drive tumor progression through CRAF. Cell **140**:209–221.
16. **Hinselwood DC, Abrahamsen TW, Ekstrom PO.** 2005. BRAF mutation detection and identification by cycling temperature capillary electrophoresis. Electrophoresis **26**:2553–2561.
17. **Johnson LN, Lowe ED, Noble ME, Owen DJ.** 1998. The Eleventh Datta Lecture. The structural basis for substrate recognition and control by protein kinases. FEBS Lett. **430**:1–11.
18. **Jung CK, et al.** 2012. Mutational patterns and novel mutations of BRAF gene in a large cohort of Korean patients with papillary thyroid carcinoma. Thyroid **22**:791–797.
19. **Karreth FA, DeNicola GM, Winter SP, Tuveson DA.** 2009. C-Raf inhibits MAPK activation and transformation by B-Raf(V600E). Mol. Cell **36**:477–486.
20. **Kobayashi T, et al.** 2010. Molecular and clinical analysis of RAF1 in Noonan syndrome and related disorders: dephosphorylation of serine 259 as the essential mechanism for mutant activation. Hum. Mutat. **31**:284–294.
21. **Kubicek M, et al.** 2002. Dephosphorylation of Ser-259 regulates Raf-1 membrane association. J. Biol. Chem. **277**:7913–7919.
22. **Leicht DT, et al.** 2007. Raf kinases: function, regulation and role in human cancer. Biochim. Biophys. Acta **1773**:1196–1212.
23. **Light Y, Paterson H, Marais R.** 2002. 14-3-3 antagonizes Ras-mediated Raf-1 recruitment to the plasma membrane to maintain signaling fidelity. Mol. Cell. Biol. **22**:4984–4996.
24. **Malumbres M, Barbacid M.** 2003. RAS oncogenes: the first 30 years. Nat. Rev. Cancer **3**:459–465.
25. **Matallanas D, et al.** 2011. Raf family kinases: old dogs have learned new tricks. Genes Cancer **2**:232–260.
26. **Molzan M, et al.** 2010. Impaired binding of 14-3-3 to C-RAF in Noonan syndrome suggests new approaches in diseases with increased Ras signaling. Mol. Cell. Biol. **30**:4698–4711.
27. **Noble C, et al.** 2008. CRAF autophosphorylation of serine 621 is required to prevent its proteasome-mediated degradation. Mol. Cell **31**:862–872.
28. **Nora JJ, Nora AH, Sinha AK, Spangler RD, Lubs HA.** 1974. The Ullrich-Noonan syndrome (Turner phenotype). Am. J. Dis. Child. **127**:48–55.
29. **O'Neill E, Rushworth L, Baccarini M, Kolch W.** 2004. Role of the kinase MST2 in suppression of apoptosis by the proto-oncogene product Raf-1. Science **306**:2267–2270.
30. **Opitz JM.** 1985. The Noonan syndrome. Am. J. Med. Genet. **21**:515–518.
31. **Pandit B, et al.** 2007. Gain-of-function RAF1 mutations cause Noonan and LEOPARD syndromes with hypertrophic cardiomyopathy. Nat. Genet. **39**:1007–1012.
32. **Piazzolla D, Meissl K, Kucerova L, Rubiolo C, Baccarini M.** 2005. Raf-1 sets the threshold of Fas sensitivity by modulating Rok-alpha signaling. J. Cell Biol. **171**:1013–1022.
33. **Poulikakos PI, Zhang C, Bollag G, Shokat KM, Rosen N.** 2010. RAF inhibitors transactivate RAF dimers and ERK signalling in cells with wild-type BRAF. Nature **464**:427–430.
34. **Pritchard CA, Bolin L, Slattery R, Murray R, McMahon M.** 1996. Post-natal lethality and neurological and gastrointestinal defects in mice with targeted disruption of the A-Raf protein kinase gene. Curr. Biol. **6**:614–617.
35. **Rajakulendran T, Sahmi M, Lefrancois M, Sicheri F, Therrien M.** 2009. A dimerization-dependent mechanism drives RAF catalytic activation. Nature **461**:542–545.
36. **Razzaque MA, et al.** 2007. Germline gain-of-function mutations in RAF1 cause Noonan syndrome. Nat. Genet. **39**:1013–1017.
37. **Ritt DA, Monson DM, Specht SI, Morrison DK.** 2010. Impact of feedback phosphorylation and Raf heterodimerization on normal and mutant B-Raf signaling. Mol. Cell. Biol. **30**:806–819.
38. **Roberts AE, et al.** 2007. Germline gain-of-function mutations in SOS1 cause Noonan syndrome. Nat. Genet. **39**:70–74.
39. **Romano D, et al.** 2010. Proapoptotic kinase MST2 coordinates signaling crosstalk between RASSF1A, Raf-1, and Akt. Cancer Res. **70**:1195–1203.
40. **Rushworth LK, Hindley AD, O'Neill E, Kolch W.** 2006. Regulation and role of Raf-1/B-Raf heterodimerization. Mol. Cell. Biol. **26**:2262–2272.
41. **Schubbert S, et al.** 2006. Germline KRAS mutations cause Noonan syndrome. Nat. Genet. **38**:331–336.
42. **Su IH, et al.** 2003. Ezh2 controls B cell development through histone H3 methylation and Igh rearrangement. Nat. Immunol. **4**:124–131.
43. **Takeda N, et al.** 2010. Cardiac fibroblasts are essential for the adaptive response of the murine heart to pressure overload. J. Clin. Invest. **120**:254–265.
44. **Tartaglia M, Gelb BD.** 2005. Noonan syndrome and related disorders: genetics and pathogenesis. Annu. Rev. Genomics Hum. Genet. **6**:45–68.
45. **Tartaglia M, Gelb BD, Zenker M.** 2011. Noonan syndrome and clinically related disorders. Best Pract. Res. Clin. Endocrinol. Metab. **25**:161–179.
46. **Tartaglia M, et al.** 2001. Mutations in PTPN11, encoding the protein tyrosine phosphatase SHP-2, cause Noonan syndrome. Nat. Genet. **29**:465–468.
47. **Tartaglia M, et al.** 2007. Gain-of-function SOS1 mutations cause a distinctive form of Noonan syndrome. Nat. Genet. **39**:75–79.

48. **Thum T, et al.** 2008. MicroRNA-21 contributes to myocardial disease by stimulating MAP kinase signalling in fibroblasts. Nature **456**:980–984.
49. **Tidyman WE, Rauen KA.** 2009. The RASopathies: developmental syndromes of Ras/MAPK pathway dysregulation. Curr. Opin. Genet. Dev. **19**:230–236.
50. **Todaro GJ, Green H.** 1963. Quantitative studies of the growth of mouse embryo cells in culture and their development into established lines. J. Cell Biol. **17**:299–313.
51. **Wan PT, et al.** 2004. Mechanism of activation of the RAF-ERK signaling pathway by oncogenic mutations of B-RAF. Cell **116**:855–867.
52. **Weber CK, Slupsky JR, Kalmes HA, Rapp UR.** 2001. Active Ras induces heterodimerization of cRaf and BRaf. Cancer Res. **61**:3595–3598.
53. **Wellbrock C, Karasarides M, Marais R.** 2004. The RAF proteins take centre stage. Nat. Rev. Mol. Cell Biol. **5**:875–885.
54. **Wu X, et al.** 2011. MEK-ERK pathway modulation ameliorates disease phenotypes in a mouse model of Noonan syndrome associated with the Raf1(L613V) mutation. J. Clin. Invest. **121**:1009–1025.
55. **Yamaguchi O, et al.** 2004. Cardiac-specific disruption of the c-raf-1 gene induces cardiac dysfunction and apoptosis. J. Clin. Invest. **114**:937–943.
56. **Zenker M, et al.** 2007. Expansion of the genotypic and phenotypic spectrum in patients with KRAS germline mutations. J. Med. Genet. **44**:131–135.
57. **Zhang SQ, et al.** 2004. Shp2 regulates SRC family kinase activity and Ras/Erk activation by controlling Csk recruitment. Mol. Cell **13**:341–355.
58. **Zobel C, Kassiri Z, Nguyen TT, Meng Y, Backx PH.** 2002. Prevention of hypertrophy by overexpression of Kv4.2 in cultured neonatal cardiomyocytes. Circulation **106**:2385–2391.